AICT 2022

The Eighteenth Advanced International Conference on Telecommunications

June 26th –30th, 2022

Porto, Portugal

AICT 2022 Editors

Sergei Semenov, HiSilicon, Sweden

AICT 2022

Forward

The Eighteenth Advanced International Conference on Telecommunications (AICT 2022), held between June 26th and June 30th, 2022, continued a series of events covering a variety of challenging telecommunication topics ranging from background fields like signals, traffic, coding, communication basics, to large communication systems and networks, fixed, mobile and integrated, etc. Applications, services, systems, and network management issues also received significant attention.

The spectrum of 21st Century telecommunications is marked by the arrival of new business models, new platforms, new architectures, and new customer profiles. Next generation networks, IP multimedia systems, IPTV, and converging network and services are new telecommunications paradigms. Technology achievements in terms of co-existence of IPv4 and IPv6, multiple access technologies, IP-MPLS network design driven methods, multicast and high speed require innovative approaches to design and develop large scale telecommunications networks.

Mobile and wireless communications add profit to large spectrum of technologies and services. We witness the evolution 2G, 2.5G, 3G and beyond, personal communications, cellular and ad hoc networks, as well as multimedia communications.

Web Services add a new dimension to telecommunications, where aspects of speed, security, trust, performance, resilience, and robustness are particularly salient. This requires new service delivery platforms, intelligent network theory, new telecommunications software tools, new communications protocols and standards.

We are witnessing many technological paradigm shifts imposed by the complexity induced by the notions of fully shared resources, cooperative work, and resource availability. P2P, GRID, Clusters, Web Services, Delay Tolerant Networks, Service/Resource identification and localization illustrate aspects where some components and/or services expose features that are neither stable nor fully guaranteed. Examples of technologies exposing similar behavior are WiFi, WiMax, WideBand, UWB, ZigBee, MBWA and others.

Management aspects related to autonomic and adaptive management includes the entire arsenal of self-ilities. Autonomic Computing, On-Demand Networks and Utility Computing together with Adaptive Management and Self-Management Applications collocating with classical networks management represent other categories of behavior dealing with the paradigm of partial and intermittent resources.

We take here the opportunity to warmly thank all the members of the AICT 2022 technical program committee, as well as all the reviewers. The creation of such a high-quality conference program would not have been possible without their involvement. We also kindly thank all the authors who dedicated much of their time and effort to contribute to AICT 2022. We truly believe that, thanks to all these efforts, the final conference program consisted of top-quality contributions. We also thank the members of the AICT 2022 organizing committee for their help in handling the logistics of this event.

We hope that AICT 2022 was a successful international forum for the exchange of ideas and results between academia and industry and for the promotion of progress in the field of telecommunications.

AICT 2022 Chairs

AICT 2022 Steering Committee

Dragana Krstic, University of Niš, Serbia
Kevin Daimi, University of Detroit Mercy, USA
Gautam Srivastava, Brandon University, Canada
Sergei Semenov, HiSilicon, Sweden

AICT 2022 Publicity Chairs

José Miguel Jiménez, Universitat Politècnica de València (UPV), Spain
Laura Garcia, Universitat Politècnica de València (UPV), Spain

AICT 2022
Committee

AICT 2022 Steering Committee

Dragana Krstic, University of Niš, Serbia
Kevin Daimi, University of Detroit Mercy, USA
Gautam Srivastava, Brandon University, Canada
Sergei Semenov, HiSilicon, Sweden

AICT 2022 Publicity Chairs

José Miguel Jiménez, Universitat Politècnica de València (UPV), Spain
Laura Garcia, Universitat Politècnica de València (UPV), Spain

AICT 2022 Technical Program Committee

Ghulam Abbas, GIK Institute, Pakistan
Iwan Adhicandra, University of Sydney, Australia
Abdullah Al-Alaj, Virginia Wesleyan University, USA
Abdulazaz Albalawi (Aziz), University of California, Santa Cruz, USA
Michele Albano, Aalborg University, Denmark
Nicolae Dumitru Alexandru, "Gheorghe Asachi" Technical University of Iasi, Romania
Marco Aurélio Spohn, Federal University of Fronteira Sul, Brazil
Ilija Basicevic, University of Novi Sad, Serbia
Oussama Bazzi, Lebanese University, Lebanon
Carlos Becker Westphall, Federal University of Santa Catarina, Brazil
Sara Behjatjamal, Altinbas University, Turkey
Stefano Berretti, University of Firenze, Italy
Robert Bestak, Czech Technical University in Prague, Czech Republic
Razvan Bocu, Transilvania University of Brasov, Romania
Antonella Bogoni, Scuola Superiore Sant'Anna-TeCIP Institute, Italy
Eugen Borcoci, University "Politehnica"of Bucharest (UPB), Romania
Christos Bouras, University of Patras, Greece
An Braeken, Vrije Universiteit Brussel, Belgium
Lubomir Brancík, Brno University of Technology, Czech Republic
Peter Brida, University of Zilina, Slovakia
Nicola Calabretta, Eindhoven University of Technology, Netherlands
Vítor Carvalho, 2Ai-EST-IPCA / Algoritmi Research Center - Minho University, Portugal
Fernando Cerdan, Polytechnic University of Cartagena, Spain
Adil Chekati, University of Tunis El Manar, Tunisia
Chen Chen, Chongqing University, China
Enrique Chirivella Pérez, Universitat de Valencia, Spain
Tanveer Choudhury, Federation University Australia, Australia
Chi-Wai Chow, National Chiao Tung University, Taiwan
Giampiero Contestabile, Scuola Superiore Sant'Anna, Pisa, Italy
Kevin Daimi, University of Detroit Mercy, USA

Laura-Maria Dogariu, University Politehnica of Bucharest, Romania
Thomas Dreibholz, SimulaMet - Simula Metropolitan Centre for Digital Engineering, Norway
Roman Dunaytsev, Saint-Petersburg State University of Telecommunications, Russia
Ashutosh Dhar Dwivedi, Technical University of Denmark, Denmark
Ersin Elbasi, American University of the Middle East, Kuwait
Mahmoud M. Elmesalawy, Helwan University, Egypt
Anna Esposito, Università della Campania "Luigi Vanvitelli", Italy
Mario Ezequiel Augusto, Santa Catarina State University, Brazil
Mário Ferreira, University of Aveiro, Portugal
Wendy Flores-Fuentes, Autonomous University of Baja California, Mexicali, Mexico
Gianluca Fontanesi, University College Dublin, Ireland
Wolfgang Frohberg, AKAD University Stuttgart, Germany
Ivan Ganchev, University of Limerick, Ireland / University of Plovdiv "Paisii Hilendarski", Bulgaria
Seema Garg, Nokia, India
Gustavo Gatica, Universidad Andres Bello, Chile
Gelayol Golcarenarenji, University of the West of Scotland, UK
Pantea Nadimi Goki, TeCIP Institute Scuola Superiore Sant'Anna, Pisa, Italy
Luís Gonçalo Cancela, ISCTE-IUL & Instituto de Telecomunicações, Portugal
Norton Gonzalez, Luciano Feijão Faculty, Sobral, Ceará, Brazil
Javier Gozalvez, Universidad Miguel Hernandez de Elche, Spain
Christian Grasso, University of Catania, Italy
Serkan Günel, Dokuz Eylül Üniversitesi, Turkey
Jan Haase, University of Lübeck, Germany
Takeshi Ikenaga, Kyushu Institute of Technology, Japan
Ilias Iliadis, IBM Research - Zurich Laboratory, Switzerland
Faouzi Jaidi, University of Carthage | Higher School of Communications of Tunis & National School of Engineers of Carthage, Tunisia
Sara Behjat Jamal, Ayvansaray University, Turkey
Vahid Joroughi, GomSpace, Denmark
Branislav Jovic, Defence Technology Agency (DTA) | New Zealand Defence Force (NZDF), Auckland, New Zealand
Kheira Kahili, ESTACA'LAB, France / LMT Lab, Algeria
Georgios Kambourakis, University of the Aegean, Greece
Dimitris Kanellopoulos, University of Patras, Greece
Arashdeep Kaur, GLBITM, Greater Noida, India
Anne Kayem, Hasso-Plattner-Institute | University of Potsdam, Germany
Hamzeh Khalili, i2CAT foundation, Barcelona, Spain
Samer Khamaiseh, Monmouth University, New Jersey, USA
David Khoury, AUST (American University of Science &Technology), Beirut, Lebanon
Uliana Kochetkova, Saint Petersburg State University, Russia
Ivan Kotuliak, Slovak University of Technology, Bratislava, Slovakia
Višnja Križanović, Josip Juraj Strossmayer Unversity of Osijek, Croatia
Dragana Krstic, University of Niš, Serbia
Hoang Le, Google, USA
Philippe Le Parc, Univesrsité de Bretagne Occidental - University of Brest, France
Gyu Myoung Lee, Liverpool John Moores University, UK
Gong-Ru Lin, National Taiwan University, Taiwan
Yu-Sheng Lin, Southern Taiwan University of Science and Technology, Tainan, Taiwan

Vincent Savaux, b-com, Rennes, France
Antonio Luiz Schalata Pacheco, Federal University of Santa Catarina, Brazil
Motoyoshi Sekiya, Fujitsu Laboratories, Japan
Sergei Semenov, HiSilicon, Sweden
Ana Serrano Tellería, University of Castilla La Mancha, Spain
A. F. M. Shahen Shah, Yildiz Technical University, Istanbul, Turkey
Yingjie Shao, The Chinese University of Hong Kong, Hong Kong
Pietro Siciliano, Institute for Microelectronics and Microsystems IMM-CNR, Lecce, Italy
Shuaib Siddiqui, Fundacio i2CAT, Barcelona, Spain
Zdenek Smekal, Brno University of Technology, Czech Republic
Antonio Sorrentino, Università Parthenope, Napoli, Italy
Gautam Srivastava, Brandon University, Canada
Kostas Stamos, University of Patras, Greece
Horia Stefanescu, Orange, Romania
Oscar Tamburis, Università "Federico II" Napoli, Italy
Mahdi Tousizadeh, University of Malaya, Malaysia
Angelo Trotta, University of Bologna, Italy
Thrasyvoulos Tsiatsos, Aristotle University of Thessaloniki, Greece
Sezer Ulukaya, Trakya University, Turkey
Rob van der Mei, Centre for Mathematics and Computer Science (CWI), Netherlands
Bernd E. Wolfinger, University of Hamburg, Germany
Xuwei Xue, Beijing University of Posts and Communications, China
Ramin Yahyapour, Georg-August-Universitaet Goettingen/GWDG, Germany
Hui Yang, Beijing University of Posts and Telecommunications (BUPT), China
Mehmet Akif Yazici, Informatics Institute - Istanbul Technical University, Turkey
Chien-Hung Yeh, Feng Chia University, Taiwan
Shaohua Yu, Northwestern Polytechnical University, China
Mariusz Zal, Poznan University of Technology, Poland
Francesco Zampognaro, University of Rome "Tor Vergata", Italy
Stefania Zinno, University of Naples Federico II, Italy
Piotr Zwierzykowski, Poznan University of Technology, Poland

Copyright Information

Table of Contents

Energy Efficiency of LoRa based Wireless Sensor Networks for Environmental Monitoring and Precision Agriculture

Višnja Križanović, Daria Ćaćić, Krešimir Grgić, Drago Žagar

Faculty of Electrical Engineering, Computer Science and Information Technology
Josip Juraj Strossmayer University of Osijek
Osijek, Croatia
email: visnja.krizanovic@ferit.hr, daria.cacic@student.ferit.hr, kresimir.grgic@ferit.hr, drago.zagar@ferit.hr

Abstract—**Sensor networks as a special subtype of wireless networks consist of a set of wirelessly connected sensor nodes. As sensor nodes have their own power sources, the network must be energy efficient, i.e., it is necessary to achieve minimal energy consumption. Therefore, energy efficiency of wireless sensor networks used for monitoring of environmental parameters is extremely important in remote networking scenarios. In this paper, an analysis of the energy consumption of sensor nodes in Long Range (LoRa) based wireless sensor networks, which are used in agriculture to observe environmental parameters, is performed. Network configuration is analyzed with regard to optimization of energy consumption in terms of selection of adequate network topologies, nodes layouts, data collection and routing processes, as well as settings of network radio parameters.**

Keywords- LoRa; Wireless Sensor Network, Environmental Monitoring; Precision Agriculture.

I. INTRODUCTION

Sensor networks as a special subtype of wireless networks consist of a set of wirelessly connected sensor nodes. The connected sensor nodes form networks used for gathering and exchanging information, and for forwarding data via gateways to public or private servers [1]. Data is then collected on storage servers for easier access and data processing [2].

Considering the fact that the sensor nodes can be equipped with different types of sensors, the field of application of wireless sensor networks is very wide. One of many possible areas of application of wireless sensor networks under Internet of Things (IoT) paradigm includes their application in agriculture and monitoring of environmental parameters [3-8]. In this case, the test environment consists of agricultural crops for which environmental and other parameters important for yield prediction are observed under different conditions. Wireless systems based on usage of sensor nodes make agricultural processes more intelligent, since they become more precise, data-oriented and highly automated [9].

The source of energy required for the operation of the sensor node is mainly a battery, which is sometimes connected to an additional system for its charging, for example with a solar collector. Replacing the battery is often impossible or impractical.

Therefore, the power supply capacity of the battery of the sensor node is one of the most severely limited resources in the wireless sensor network. Moreover, for implementation of the wireless sensor network, it is important to take into account the optimization of energy consumption and to achieve maximum possible energy savings [10].

Therefore, in this paper, an analysis of configurations of wireless sensor networks is carried out with regard to optimization of energy consumption. Optimization is analyzed in terms of selection of adequate topologies, node layouts, data collection and routing processes, as well as settings of network radio parameters. In Section II, selection of network technology used in further analysis is explained. In Section III, a comparative overview of energy consumption for different topologies of wireless sensor networks is presented. In Section IV, an analysis of adequate methods for data collection is performed. In Section V, additional analysis of configurations of radio parameters is conducted to select solutions that have appropriate range and energy efficiency.

II. SELECTION OF NETWORK TECHNOLOGY

Sensor nodes are characterized by small dimensions, low energy consumption, the ability to collect data via appropriate sensors, the ability to process data, and to support wireless communication within appropriate range. This concept enables the collection of data very close to the observed area, local aggregation of data and easy transfer of data to remote central locations intended for data collection and processing. Wireless sensor networks may contain a number of nodes located at relatively short distances from each other. Communication between nodes, as well as communication of nodes with the gateway can take place directly or through multiple nodes, within the so-called multi-hop topology, topology which extends the communication range [11].

Analyses of various aspects of wireless sensor networks implemented in rural environment are conducted hereafter to optimize operating parameters from the communications point of view. Optimization of wireless communication parameters is carried out with an aim of achieving fast and reliable communication with minimal energy consumption. Optimization is important for processes of directing the collected sensor data to a remote distant destination.

For use in agriculture and monitoring of environmental parameters, sensor networks are placed in remote locations, i.e., test fields. Therefore, it is necessary to use networking technologies that can achieve connectivity over long distances up to several tens of kilometers. For this reason, the application of short-range communication technologies (e.g., WiFi and ZigBee) is not suitable due to installation barriers of additional gateways, lack of suitable locations or inadequate electricity connectivity [12]. Although the deployment of communication via mobile networks meets the requirements on range and reliability, it is energy demanding and incurs additional costs in terms of a permanent subscriptions to the service provider. Hence, it is also not an optimal solution [13]. In addition to long range, the next important criterion in the selection of appropriate technologies is low energy consumption, so that the battery-powered nodes achieve a sufficiently long autonomy and multi-year life expectancy. Therefore, technologies from the group of Low Power Wide Area Network (LPWAN) technologies are suitable for application in precision agriculture scenarios [14]. LPWAN is the name for high-range, low-power wireless technologies. The specifics of LPWAN technologies are low power consumption and long communication range for sending information over greater distances. These features make LPWAN technologies very practical for open area IoT implementations. There are many LPWAN technologies and new ones are constantly emerging and improving, but currently LoRa, Sigfox and Narrowband IoT (NB-IoT) are leaders in this field [15,16]. The advantage of application of these technologies in networking relates to the fact that the end devices working with these technologies are designed to consume energy efficiently and minimally [17]. Low power and narrow bandwidth allow very low power consumption when sending messages [18]. Due to the simplicity of LoRa deployment in the fields, this paper analyzes the application of LoRa in agriculture for monitoring environmental parameters and optimization of its energy consumption in related scenarios. Considering the range of communication, LoRa has sufficient range required for its application in rural areas [9].

III. SELECTION OF NETWORK TOPOLOGIES

Through simulation procedures, networking scenarios using LoRa technology are analyzed. In these scenarios, sensor nodes communicate via a gateway with the rest of the network. The *CupCarbon* IoT simulator [19] is used for simulation and analysis of energy consumption during communication processes. For comparing topologies and selecting appropriate network topologies, a star topology is suitable for many and diverse IoT applications. However, in a number of scenarios, a more flexible network topology like decentralized multi-hop solution is needed [11]. Therefore, in order to compare the network topologies from the aspect of energy consumption, the star topology, i.e., one-hop topology, and topology in which linear structures are formed in clusters, i.e., multi-hop linear topologies, are selected, as shown in Figures 1 and 2. The terminal devices in the access network are sensor nodes.
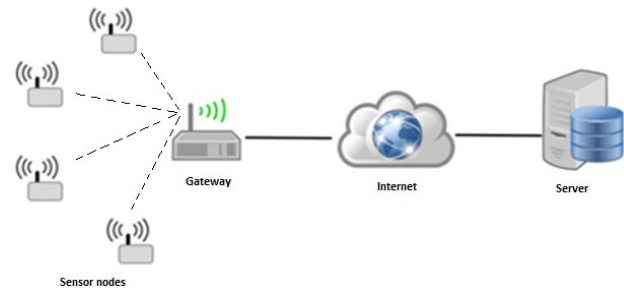
Figure 1.   Star topology (one-hop).
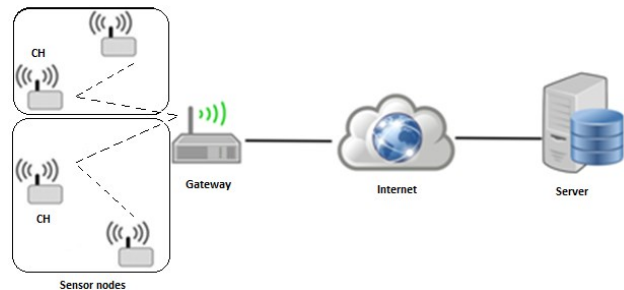
Figure 2.   Line topology within individual clusters (multi-hop).

As presented in Figures 1 and 2, sensors measure data sent to the rest of the network via a gateway. Terminal devices, i.e. sensor nodes, rely on the gateway to transmit information from the access network to the network server.

A. Star topology

To start the analysis of energy consumption in different access network topologies, the star topology, topology in which each sensor node sends data directly to the gateway is chosen. The star topology is convenient for its ease of deployment.

Figure 3 shows the access part of the network created in the *CupCarbon* IoT simulator which includes the sensor nodes, marked as *s2* to *s5*, connected to the gateway. Figure 3 also shows the radii of area coverage with signal for individual nodes, which depend on the area range each node needs to cover with its signal. Thus, for example, node *s4* needs a smaller signal coverage radius for covering the area up to the gateway, while node *s2* needs a larger signal coverage radius so that the gateway can be reached, as presented in Figure 3. The ranges of area coverage with signal can be defined through an *atpl* parameter, which defines the percentage of signal coverage for each node in relation to the maximum possible coverage area, as defined in Table I for nodes *s4* and *s5*. In the case when the specified parameter is not defined for the node, it is considered that the node covers the maximum possible area it can cover with its signal. As presented in Table I, the gateway waits for the data to be sent from the sensor nodes according to the randomly selected (*randb*) moment for data sending that has a certain time delay.
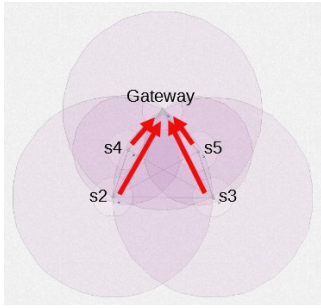
Figure 3. Representation of communication between nodes in scenario with star topology.

Figure 5. Representation of communication between nodes in scenario with line topology within clusters and with CH nodes closest to the gateway

Figure 3 shows the star topology and communication among nodes in the access network. The illustration shows that the sensor nodes (*s2*, *s3*, *s4* and *s5*) send data directly to the gateway. This is defined through a *send* parameter that defines which node sends data to which one. Thus, for example, the label *send 1 1* in Table I defines that nodes *s2*, *s3*, *s4* and *s5* send one data packet to node 1, i.e., the gateway. The *randb* parameter is used to send data with a random delay variable *x*. In order to compare the topologies that can be used in communication between sensor nodes and the gateway, power consumption in the example of a star network topology is presented in Fig 4. According to the level of energy consumption shown in Figure 4, it can be seen that the sensor nodes closer to the gateway, i.e., *s4* and *s5*, consume less energy than the more distant nodes, i.e., *s2* and *s3*. Further comparison of the results obtained should be possible when the results for different topologies are taken into account within a similar time period as indicated on the abscissa.

Figure 4. Energy consumption of LoRa technology in scenario with star topology.

TABLE I. PARAMETERS CONFIGURATION FOR STAR TOPOLOGY

Nodes	Nodes marking:		
	Gateway:	*s2* and *s3*:	*s4* and *s5*:
Instruct.:	loop wait read x	loop randb x 10 1000 delay $x send 1 1 delay 50	loop atpl 55 randb x 10 1000 delay $x send 1 1 delay 50

B. Multi-hop linear topology

Next, the topologies in which linear structures are formed in individual clusters, i.e., multi-hop linear topologies, are analyzed. Unlike in mesh, in these topologies network data collision issues could be mitigated so they are selected for the analysis of reliable network data transmission.

1) Line topology within clusters with CH nodes closest to the gateway

In the combination of line network topologies presented in Figure 5, some sensor nodes within individual clusters can communicate with each other, e.g., *s2* and *s4*, as well as *s3* and *s5*. The so-called *Claster Head* (CH) nodes, nodes *s4* and *s5*, communicate directly with the gateway. They rely on the gateway to transmit information to the network server, as shown in Figure 5. The other nodes, *s2* and *s3*, forward data in the direction of CH nodes. Devices are synchronized and wake up at specific moments in time to receive data packets from their neighbors, which they can combine with their own data packets and send further along the line. This scenario is created considering the conclusion given for the star topology that the distance of the nodes affects the energy consumption. Therefore, for the CH node within each cluster, the node closest to the gateway within the cluster is selected and its choice is fixed throughout the simulation process of network data transmission.

Figure 5 illustrates the determined signal coverage radii for individual nodes. They depend on the range each sensor node needs to have to cover the area with its signal. In this scenario, it is assumed that, in order to cover the area up to the gateway, node *s4* needs the same signal coverage radius as node *s2* in order to reach node *s4*. The reason is a comparison of the impact of different frequencies of data transmission of nodes on energy consumption. From Figure 5 it can be seen that sensor nodes *s2* and *s3* send data to nodes *s4* and *s5*. The nodes *s4* and *s5* then send their data, as well as data received from nodes *s2* and *s3*, directly to the gateway. The two clusters with line communication within nodes are created, one with *s2* and *s4*, and one with *s3* and *s5*, in which the CH nodes are nodes *s4* and *s5*. According to the configuration of the parameters of nodes, it can be seen that the specified ranges of signal coverage are also defined through the *atpl* parameter.

TABLE II.　　PARAMETERS CONFIGURATION FOR LINE TOPOLOGY WITHIN CLUSTERS WITH CH NODES CLOSEST TO THE GATEWAY

Nodes	Nodes marking:			
	Gateway:	*s2:*	*s3:*	*s4* and *s5:*
Instructions:	*loop* *wait* *read x*	*loop* *atpl 55* *randb x 10 1000* *delay $x* *send 1 4* *delay 50*	*loop* *atpl 55* *randb x 10 1000* *delay $x* *send 1 5* *delay 50*	*loop* *atpl 55* *randb x 10 1000* *delay $x* *send 1 1* *delay 50* *send 1 1* *delay 50*

For each node, the percentage of coverage area in relation to the maximum possible coverage area of the node is defined as presented in Table II for nodes *s2*, *s3*, *s4* and *s5*. From Table II, it can be seen that nodes *s4* and *s5* need the same signal coverage radius for covering area up to the gateway, as radius of node *s2* to reach node *s4*, as well as radius of node *s3* to reach node *s5*. According to the level of energy consumption shown in Figure 6, it is evident that node *s2* sends data more often than node *s3*, so its energy consumption is higher. The CH nodes, i.e., nodes *s4* and *s5*, although the closest to the gateway, consume more energy than the more distant nodes, i.e., nodes *s2* and *s3*. The reason for this is the fact that CH nodes receive data from nodes *s2* and *s3*, and send them to the gateway along with their own data. The gateway waits for the data sent from the CH nodes according to the randomly selected moment for sending with a certain time delay. In this scenario, the total energy consumption is higher than in the star topology.

2) Line topology within clusters with CH nodes furthest from the gateway

To avoid fast energy depletion of CH nodes selected in a fixed manner, this scenario gives the analysis of energy consumption of randomly selecting CH nodes, and not fixed ones, as in the previous example. In the combination of line network topologies within individual clusters shown in Figure 7, sensor nodes can communicate with each other, e.g., *s2* and *s4*, as well as *s3* and *s5*. For CH nodes, the data transmission process relies on the gateway to transmit information to the network server. In this example, the CH nodes are selected at random.

Figure 6.　Energy consumption of LoRa technology in scenario with line topology within clusters and with CH nodes closest to the gateway.
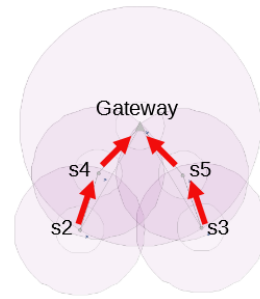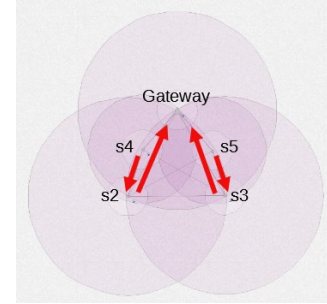

Figure 7.　Representation of communication between nodes in scenario with line topology within clusters and with CH nodes furthest from the gateway.

For the CH node within each cluster at one point, as well as the nearest, the nodes furthest from the gateway can be selected, i.e., nodes *s2* and *s3*. In Figure 7, the signal coverage radii for individual nodes are shown, depending on the area ranges that the nodes need to cover with their signal. Thus, for example, node *s4* needs a smaller signal coverage radius covering the area up to node *s2*, compared to the necessary radius of node *s2* for reaching the gateway. The same is true for the radii of nodes *s3* and *s5*.

According to the level of energy consumption shown in Figure 8, it can be seen that the sensor CH nodes, i.e., nodes *s2* and *s3*, furthest from the gateway, consume more energy than nodes *s4* and *s5*. At one point, nodes *s4* and *s5* send their data to the CH nodes *s2* and *s3*, which then send these data to the gateway in addition to their own data.

For a comparison with the energy consumption in the example of a line topology within a cluster with CH nodes closest to the gateway, a much higher energy consumption of CH nodes can be noted in this scenario. Moreover, the comparison of the results from Figures 4, 6, and 8 shows that in a star topology, unlike multi-hop topologies, the optimal scaling strategy of LoRa radio parameters can be achieved to obtain the long range communication while enabling the lowest energy consumption.

As defined in Table III for nodes *s4* and *s5*, the specified ranges of signal coverage radii are also defined through the *atpl* parameter. There is also the case when the specified *atpl* parameter is not defined for the node. In this case, it is considered that the node covers the maximum possible area that it can with its signal. This is the case for nodes *s2* and *s3*. This allows for random selection of CH nodes as each node, from *s2* to *s5*, is able to cover the area to the gateway with its signal.

The random choice of CH nodes was selected in this scenario to analyze the possibility of reducing the energy depletion of certain CH nodes selected in a fixed manner, as it was the case in the previous scenario with the fastest energy depletion of CH nodes selected in a fixed manner, i.e., the ones closest to the gateway. However, the total amount of energy consumed within the observed time period in this scenario is the highest.
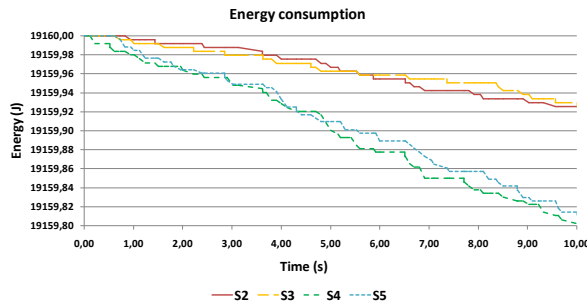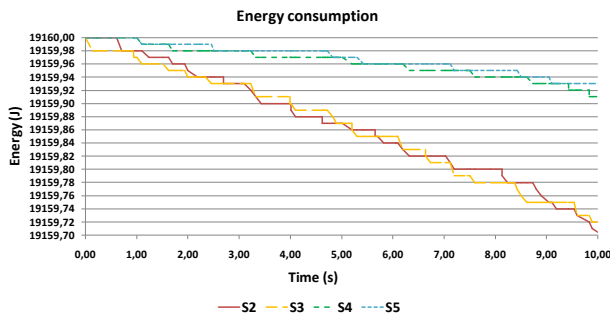
Figure 8.   Energy consumption of LoRa technology in scenario with line topology within clusters and with CH nodes furthest from gateway.

TABLE III.   PARAMETERS CONFIGURATION FOR LINE TOPOLOGY WITHIN CLUSTERS WITH CH NODES FURTHEST FROM THE GATEWAY

Nodes	Nodes marking:			
	Gateway:	*s2* and *s3*:	*s4*:	*s5*:
Instructions:	*loop* *wait* *read x*	*loop* *randb x 10 1000* *delay $x* *send 1 1* *delay 50* *send 1 1* *delay 50*	*loop* *atpl 55* *randb x 10 1000* *delay $x* *send 1 2* *delay 50*	*loop* *atpl 55* *randb x 10 1000* *delay $x* *send 1 3* *delay 50*

From the comparison of the results in Figures 4, 6, and 8 it can be concluded that the star network topology can be considered as the best option with regard to cumulative energy consumption.

IV.   SELECTION OF ADEQUATE VOLUME OF NETWORK TRAFFIC

The following scenarios are created with the aim of analyzing the impact of the amount of transmitted network traffic within the network on the energy consumption in the network. These scenarios aim to reduce energy consumption with adequate traffic volume, and to improve the range. The energy consumption control is considered and the rate adaptation for one-hop scenarios presented in Figure 9 is analyzed. For this purpose, the network topology shown in Figure 9 was created, which consists of sensor nodes, marked *s2* to *s7*, and a remote gateway. Star topology is used for communication between nodes.
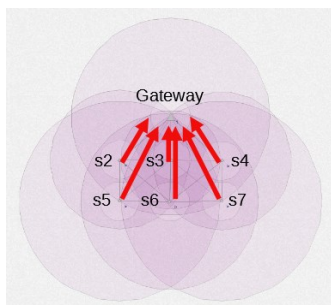
Figure 9.   Communication between nodes for one-hop scenarios.

In previous examples, the star topology was defined as more appropriate in terms of total energy consumption compared to the line structure within clusters. The radii of area coverage with signal for individual nodes are shown in Figure 9, so the node closest to the gateway has the smallest radius, i.e., node s3, while the nodes furthest from the gateway, i.e., nodes s5 and s7, have the largest radii.

A.   Sending an equal amount of traffic from nodes equally distant from the gateway

As shown in Table IV, in this scenario, the gateway waits for data to be sent from the sensor nodes *s2* to *s7* and then reads the sent data *x* and proceeds with data forwarding.

The largest radius for data transmission is used by nodes *s5* and *s7*, which can be seen according to the omitted parameter *atpl* in Table IV. This implies usage of the entire available coverage radii of the nodes *s5* and *s7*. This parameter is specified for nodes *s2*, *s3*, *s4* and *s6*. It can be seen that node *s3* uses the smallest radius (50% of the total largest possible radius). Data is sent continuously (*loop*), but a delay is made between sending individual data. This scenario corresponds to predefined data transmission moments in which all nodes send data at the same time intervals. This is a common case in rural scenarios for sending data collected from the field.

Figure 10 shows the energy consumption when applying LoRa technology in a star network topology with the same amount of data sent from nodes equally distant from the gateway. Therefore, the same amount of data is sent from nodes *s2* and *s4*, and the same amount of data from nodes *s5* and *s7*, so there are overlaps on the graph in energy consumption for these nodes. The node closest to the gateway, node *s3* consumes the least energy for sending, while the most energy is consumed by the farthest nodes, nodes *s5* and *s7*, whose energy will be depleted the fastest.
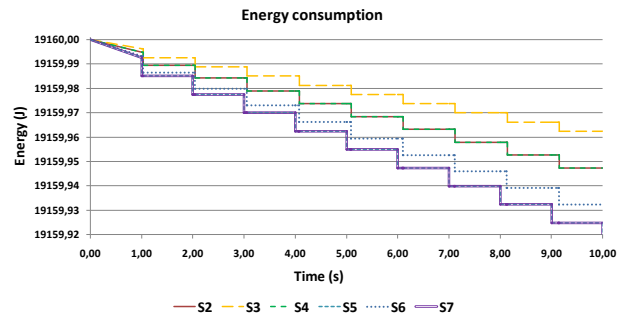
Figure 10. Energy consumption in a star topology with the same amount of data sent from nodes equally distant from the gateway.

TABLE IV.   INITIAL PARAMETERS CONFIGURATION FOR DATA TRANSMISSION

Nodes	Nodes marking:				
	Gateway:	*s2* and *s4*:	*s3*:	*s5* and *s7*:	*s6*:
Instr.:	*loop* *wait* *read x*	*loop* *atpl 70* *send 1 1* *delay 1000*	*loop* *atpl 50* *send 1 1* *delay 1000*	*loop* *send 1 1* *delay 1000*	*loop* *atpl 90* *send 1 1* *delay 1000*

TABLE V.   PARAMETERS CONFIGURATION FOR MORE FREQUENT DATA TRANSMISSION

Nodes	Nodes marking:						
	Gateway:	*s2:*	*s3:*	*s4:*	*s5:*	*s6:*	*s7:*
Instruct:	*loop wait read x*	*loop atpl 70 send 1 1 send 1 1 delay 1000*	*loop atpl 50 send 1 1 delay 1000*	*loop atpl 70 send 1 1 delay 1000*	*loop send 1 1 delay 1000*	*loop atpl 90 send 1 1 delay 1000*	*loop send 1 1 delay 1000*

TABLE VI.   PARAMETERS CONFIGURATION FOR LESS FREQUENT DATA TRANSMISSION

Nodes	Nodes marking:						
	Gateway:	*s2:*	*s3:*	*s4:*	*s5:*	*s6:*	*s7:*
Instruct.:	*loop wait read x*	*loop atpl 70 send 1 1 send 1 1 delay 2000*	*loop atpl 50 send 1 1 delay 2000*	*loop atpl 70 send 1 1 delay 2000*	*loop send 1 1 delay 2000*	*loop atpl 90 send 1 1 delay 2000*	*loop send 1 1 delay 2000*
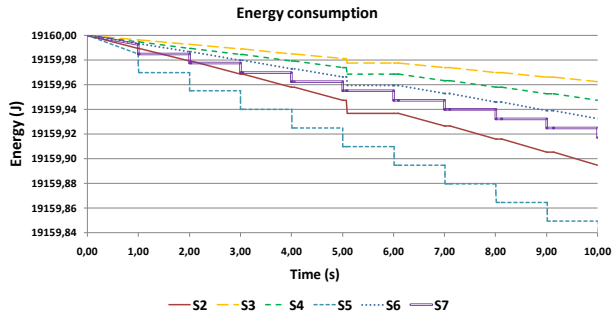
Figure 11. Energy consumption in a star topology with different amounts of data sent from nodes equally distant from the gateway.

Figure 12. Energy consumption of LoRa technology in a star topology with the less frequent sending of data from sensor nodes to the gateway.

It can be concluded that node placement in star topology presents an important determinant of sensor node life time. However, although the nodes should be as close as possible to the gateway to reduce energy consumption, at the same time, adequate coverage of area with the signal must be achieved. With regard to the energy depletion of individual nodes, the star topology is more suitable for application in sensor networks than a cluster topology

In cluster topology, the energy of CH nodes is depleted the fastest. CH nodes are difficult to replace, which causes the loss of functionality of the entire cluster, while in a star topology, the depletion of energy of an individual node does not cause such a loss in data delivery from the area which it covers with its signal.

B.   Sending different amounts of traffic from nodes equally distant from the gateway

The parameters listed in Table V are similar to the data from the previous scenario, except that data from some nodes is sent more frequently. Despite the same distance of nodes *s2* and *s4* from gateway, more data is sent from node *s2* to the gateway than from node *s4*. Moreover, from node *s5* data is sent to the gateway more often than from node *s7*, although both nodes are equally distant from the gateway. Figure 11 shows the energy consumption when applying LoRa technology in a star network topology with different amounts of data sent from nodes equidistant from the gateway. Therefore, different amount of data is sent from nodes *s2* and *s4*, and different amount of data from nodes *s5* and *s7*, so there are no overlaps on the graph in energy consumption for these nodes. The node closest to the gateway, node *s3* consumes the least energy required for sending. The most energy is consumed by the farthest node *s5*. Moreover, it sends more data compared to node *s7*, which is at the same distance from the gateway as node *s5*.

The node *s5* consumes more energy than node *s7*. From the results, it can be concluded that in scenarios where sending a larger amount of data is not necessary, as in the case of monitoring the state of yield, energy savings should be achieved by sending an adequately determined smaller volume of data from sensors.

C.   Less frequent data transmission

The parameters listed in Table VI are similar to the data from the previous scenario, except that data from nodes is sent less frequently, which is seen by a higher value of the delay parameter that defines the time delay between sending individual data. In this scenario, data is sent twice as rarely compared to the previous scenario.

Figure 12 shows the energy consumption using LoRa network access and star network topology. In this scenario, less frequent sending of data from sensor nodes to gateway is analyzed and compared with the scenario presented in Figure 11. From the comparison of the presented results, significantly less energy consumption can be noted within the same time interval when sending data with higher delay, i.e., less frequently. LoRa technology has adequate features for usage in wireless sensor networks if long-range communication with minimal power consumption should be achieved. LoRa supports data transmission with lower requirements for high transfer speeds and transfer of large amounts of data. Thus, as can be concluded from the presented results, the application of LoRa technology is an adequate solution in IoT scenarios where fast transmission of large amounts of data is not required, as in precision agriculture, where additional energy savings can be achieved by sending smaller amounts of data over longer periods of time between transmissions.

D. Effect of SF and CR parameters on Consumed Energy

The LoRa access based wireless sensor network implemented in the field serves to connect sensor nodes located in different remote locations to centrally located storage and advanced data processing servers. The communication should be achieved in an energy efficient way. It can be highlighted that the range of communication in the fields and open spaces presents one of the most important parameters because it is necessary to ensure energy efficient transmission of data over relatively long distances. In that case, the high data transfer rate is not so significant. The parameters described hereafter, the spreading factor and the coding rate, affect transmission range and energy efficiency.

The Spreading Factor (SF) presents the number of chips per symbol. Its value is an integer number between 6 and 12. The greater the SF value, the more capability the receiver has to move away the noise from the signal. Thus, the greater the SF value, the more time is taken to send a packet, but a higher range will also be achieved because the sensitivity of the receiver is better. Thus, for example, if the expansion factor is minimal, i.e., SF = 6, a higher speed can be achieved, but with a reduction in the possible range.

The expression for Coding Rate (CR) is CR =4/(4+n), where n is a value from 1 to 4. It denotes that each four useful bits are encoded by 5, 6, 7 or 8 transmission bits. The smaller the coding rate is, the higher the time on air is to transmit data. Prolonged data transfer time will also affect battery consumption.

The analysis of the effect of different values of SF and CR LoRa radio parameters on consumed energy and range is performed hereafter.

As already stated, when the SF value is high, the time for data transmission increases which means that the sensor node consumes more power to transmit data. As presented in Figure 14, the SF expansion factor is set to a maximum value of 12, unlike in the case shown in Figure 13 where the SF is set to a value of 7. The reason for setting a high SF value is to maximize the transmission range as one of the most important factors in the field deployments.

Furthermore, when the coding rate increases, the data transmission time and the consumed energy decrease. Therefore, in the case when a long range needs to be ensured, energy consumption can be regulated by the CR factor, as presented in Figures 13 and 14. The energy consumption shown in Figure 14 would have been higher if the same CR factor had been used as in the example shown in Figure 13. By increasing the CR value from 4/8 to 4/5, energy consumption can be reduced while maintaining the maximal range enabled by the high SF parameter value.

V. CONCLUSION

LoRa technology can be applied in agriculture to monitor environmental parameters. It is used for communication among remote sensor nodes located in test fields in order to achieve energy efficient communication. The LoRa system aims at pushing optimization of energy consumption further while maintaining a long range, hence the scenarios for implementation of LoRa solutions in precision agriculture have been analyzed in this paper. LoRa sensor network implementation for monitoring of environmental parameters in agriculture is analyzed.

The specifics of LoRa technology are low power consumption and long communication range used in sending information over large distances.

TABLE VII.   PARAMETERS CONFIGURATION FOR SF=7 AND CR=4/8

Nodes	Nodes marking:				
	Gateway:	s2 and s4:	s3:	s5 and s7:	s6:
Instructions:	loop wait read x	loop atpl 70 send 1 1 7 8 randb x 10 1000 delay $x send 1 1 7 8 delay 1000	loop atpl 50 send 1 1 7 8 randb x 10 1000 delay $x send 1 1 7 8 delay 1000	loop send 1 1 7 8 randb x 10 1000 delay $x send 1 1 7 8 delay 1000	loop atpl 90 send 1 1 7 8 randb x 10 1000 delay $x send 1 1 7 8 delay 1000

TABLE VIII.   PARAMETERS CONFIGURATION FOR SF=12 AND CR=4/5

Nodes	Nodes marking:				
	Gateway:	s2 and s4:	s3:	s5 and s7:	s6:
Instructions:	loop wait read x	loop atpl 70 send 1 1 12 5 randb x 10 1000 delay $x send 1 1 12 5 delay 1000	loop atpl 50 send 1 1 12 5 randb x 10 1000 delay $x send 1 1 12 5 delay 1000	loop send 1 1 12 5 randb x 10 1000 delay $x send 1 1 12 5 delay 1000	loop atpl 90 send 1 1 12 5 randb x 10 1000 delay $x send 1 1 12 5 delay 1000

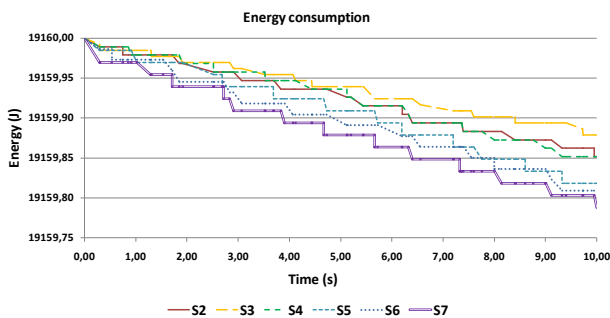Figure 13. Energy consumption of LoRa technology in a star topology with SF=7, and CR=4/8.
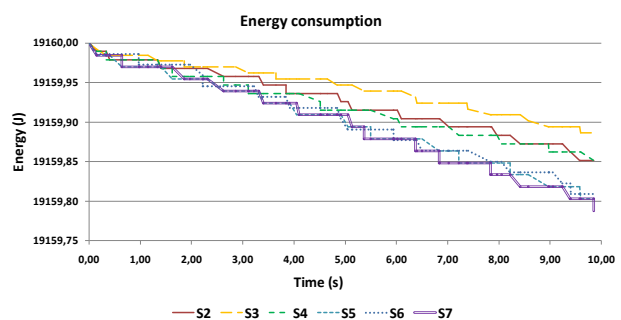

Figure 14. Energy consumption of LoRa technology in a star topology with SF=12, and CR=4/5.

The biggest drawback is the low speed of data transmission and the limited amount of data that can be sent. For LoRa based environmental monitoring, high throughput and high transfer rate are not of great importance since, generally, small amounts of data is transmitted. Basically, mainly numerical values representing readings of different types of sensors that monitor plant parameters and their close environment are sent. Therefore, it is important to achieve long-range communication with minimal energy consumption, with lower requirements for the amount and frequency of data transfer.

In this paper, LoRa star, i.e., one-hop, and multi-hop linear topologies have been compared. Considering cumulative energy consumption of sensor nodes in the network, the star topology is identified as the one which could better fit lower energy consumption in the presented scenarios. Moreover, the presented simulation results show that, for a star topology, optimal scaling strategy of LoRa radio parameters necessary for environmental monitoring can be achieved to obtain the long range while enabling low energy consumption. The presented results show that optimizing LoRa parameters, such as SF and CR, with regard to the required long range communication is a key element to reduce the consumed energy by the sensor nodes. Since the SF factor must have the highest possible value to achieve a greater range of communication necessary for precision agriculture, the presented results show that in that case the CR should be as high as possible to reduce total energy consumption. The presented findings of the effect of the studied network elements on the energy consumption collected through conducted simulations are important for further research activities in the field of LoRa based environmental monitoring and precision agriculture in rural areas.

For a multi-hop linear topologies, energy consumption can also be optimized by applying different radio configurations for different network layouts. In these topologies, the density of nodes plays a determinant role in coverage and number of hops. Therefore, future work will include analysis of optimization of energy consumption in multi-hop networks by exploiting various radio configurations and the network topologies (e.g., the number of hops, the network density, the coverage), and a strategy to take advantage of combination of both star and multi-hop topologies will be proposed.

REFERENCES

[1] K. Foughali, K. Fathallah, and A. Frihida, "Using cloud IoT for disease prevention in precision agriculture," Procedia Computer Science, vol. 130, pp. 575-582, 2018

[2] F. Karim, F. Karim, and A. Frihida, "Monitoring system using web of things in precision agriculture," Procedia Computer Science, vol. 110, pp. 402-409, 2017

[3] M. S. Farooq, S. Riaz, A. Abid, K. Abid, and M. A. Naeem, "A survey on the role of IoT in agriculture for the implementation of smart farming," IEEE Access, vol. 7, pp. 156237-156271, 2019

[4] O. Elijah, T. A. Rahman, I. Orikumhi, C. Y. Leow, and N. Hindia, "An overview of Internet of Things (IoT) and data analytics in agriculture: benefits and challenges," IEEE Internet of Things Journal, vol. 5, no. 5, pp. 3758-3773, 2018

[5] J. Chen and A. Yang, "Intelligent agriculture and its key technologies based on Internet of Things architecture," IEEE Access, vol. 7, pp. 77134-77141, 2019

[6] N. Ahmed, D. De, and I. Hussain, "Internet of Things (IoT) for smart precision agriculture and farming in rural areas," IEEE Internet of Things Journal, vol. 5, pp. 4890-4899, 2018

[7] M. Ayaz, M. Ammad-Uddin, Z. Sharif, A. Mansour, and E.-H. M. Aggoune, "Internet-of-Things (IoT)-based smart agriculture: toward making the fields talk," IEEE Access, vol. 7, pp. 129551-129583, 2019

[8] A. Khanna and S. Kaur, "Evolution of Internet of Things (IoT) and its significant impact in the field of precision agriculture," Computers and Electronics in Agriculture, vol. 157, pp. 218-231, 2019

[9] K. Grgić, D. Žagar, J. Balen, and J. Vlaović, "Internet of Things in Smart Agriculture - Possibilities and Challenges", Proceedings of the International Conference on Smart Systems and Technologies, pp. 239-244, 2020

[10] A. Tzounis, N. Katsoulas, T. Bartzanas, and C. Kittas, "Internet of Things in agriculture, recent advances and future challenges," Biosystems Engineering, vol. 164, pp. 31-48, 2017

[11] R. P. Centelles, F. Freitag, R. Meseguer, and L. Navarro "Beyond the Star of Stars: an Introduction to Multi-Hop and Mesh for LoRa and LoRaWAN", IEEE Pervasive Computing, vol. 20, pp. 63-72, 2021

[12] C. T. Kone, A. Hafid, and M. Boushaba, "Performance management of IEEE 802.15.4 wireless sensor network for precision agriculture," IEEE Sensors Journal, vol. 15, pp. 5734-5747, 2015

[13] L. Chettri, "A comprehensive survey on Internet of Things (IoT) toward 5G wireless systems," IEEE Internet of Things Journal, vol. 7, pp. 16-32, 2020

[14] U. Raza, P. Kulkarni, and M. Sooriyabandara, "Low power wide area networks: an overview," IEEE Communications Surveys & Tutorials, vol. 19, pp. 855-873, 2017

[15] K. Mekki, E. Bajic, F. Chaxel, and F. Meyer, "A comparative study of LPWAN technologies for large-scale IoT deployment," ICT Express, vol. 5, pp. 1-7, 2019

[16] R. S. Sinha, Y. Wei, and S.-H. Hwang, "A survey on LPWA technology: LoRa and NB-IoT," ICT Express, vol. 3, pp. 14-21, 2017

[17] J. P. S. Sundaram, W. Du, and Z. Zhao, "A survey on LoRa networking: research problems, current solutions, and open issues," IEEE Communications Surveys & Tutorials, vol. 22, pp. 371-388, 2020

[18] J. Xu, J. Yao, L. Wang, Z. Ming, K. Wu, and L. Chen, "Narrowband Internet of Things: evolutions, technologies, and open issues," IEEE Internet of Things Journal, vol. 5, pp. 1449-1462, 2018

[19] CupCarbon IoT Simulator, http://cupcarbon.com, [retrieved: May, 2022]

Comparison of Code Constructions Suitable for High-Throughput Decoding

Sergei Semenov

HiSilicon

Lund Research Center, Sweden

e-mail: sergei.semenov@huawei.com

Jiye Liang

HiSilicon

Beijing, China

e-mail: liangjiye@huawei.co

Mingxu Zhang

HiSilicon

Beijing, China

e-mail: zhangmingxu2@hisilicon.com

Abstract—**Two classes of codes allowing high-throughput decoding: Spatially Coupled Low Density Parity-Check (SC-LDPC) codes and staircase codes are compared. Accumulate Repeat-Jagged (ARJ)-based SC-LDPC codes provide better performance and lower complexity for Soft-Decision Decoding (SDD). However, the serious drawback of this construction is the severe performance degradation with code rate increase. The decoding complexity of SDD might still be too high to provide very high throughput. Reed-Solomon (RS)-based staircase codes under Hard-Decision Decoding (HDD) provide quite good performance with low decoding complexity. Moreover, the performance changes very smoothly with code rate increase.**

Keywords-SC-LDPC codes; Generalized Product Codes; staircase codes; high-throughput decoding.

I. INTRODUCTION

Future Beyond-5G use cases are expected to require wireless speeds in the Terabit/s range. This sets a number of tough challenges on the physical layer and especially on the Forward Error Correction (FEC). The code constructions used in current 3GPP specs can hardly be used to provide this level of throughput under channel conditions considered in use cases. Apparently, some specific requirements should be applied to the choice of a code construction allowing high throughput decoding. The decoding complexity should be low enough and the decoding algorithm should be suitable for a high level of parallelization. Especially useful for high throughput decoding are codes with high *locality* property allowing the decoder to use structures that are independent of code length in terms of complexity, storage requirements and latency.

Spatially coupled codes are known for both high locality and high performance. In this paper, we are comparing two code constructions, one of which represents the class of SC-LDPC codes and another the Generalized Product Codes (GPC). The comparison is done not only in terms of performance/complexity, but also the ability to create the code family that can be easily adapted to different code rates is considered.

The rest of this paper is organized as follows. Section II describes the code constructions considered in this paper.

Section III describes the decoding of the considered codes. Section IV addresses the comparison of the considered code constructions with the focus on ability to provide high throughput. The conclusions close the article.

II. CONSIDERED CODE CONSTRUCTIONS

The main principle of spatial coupling is that the codewords $\mathbf{v}_t$ of the block code defined by the parity-check matrix $\mathbf{H}$, instead of being encoded independently, are interconnected (coupled) with their neighbors at times $t - 1, t - 2, \ldots, t - w$ during the encoding procedure. This is done in such a way that the sequence satisfies the condition

$$\mathbf{v}_t\mathbf{H}_0^T(t) + \mathbf{v}_{t-1}\mathbf{H}_1^T(t) + \cdots + \mathbf{v}_{t-w}\mathbf{H}_w^T(t) = \mathbf{0}, \quad (1)$$

where matrices $\mathbf{H}_0(t), \mathbf{H}_1(t), \ldots, \mathbf{H}_w(t)$ result from the decomposition of the original matrix $\mathbf{H}$ [6]:

$$\mathbf{H}_0(t) + \mathbf{H}_1(t) + \cdots + \mathbf{H}_w(t) = \mathbf{H}, \quad \forall t. \quad (2)$$

It is easy to verify that both code constructions considered in this paper satisfy (1) and (2), therefore, they define spatially coupled codes.

A. SC-LDPC codes

The idea of SC-LDPC codes was proposed in [1]. It can be interpreted as generalization of block and convolutional coding where the convolutional coding is applied to the words of some block code rather than to information symbols. One of the possible ways of constructing SC-LDPC codes is constructing with the help of coupling of protographs. Recall that a protograph can be considered as a graph representing the general structure of a graph-based code, e.g., LDPC code. A protograph can be represented with the help of a Base-Graph (BG) matrix $\mathbf{B}$ where the element $b_{i,j}$ shows the number of edges connecting Check Node (CN) i and Variable Node (VN) j in the protograph. The base-graph matrix $\mathbf{B}$ can be translated to the parity-check matrix $\mathbf{H}$ by substituting each element in $\mathbf{B}$ by the corresponding permutation matrix of size $(M \times M)$, where M is the code lifting size. If the number of edges connecting CN i and VN j is more than 1 and ,e.g., is

equal to k, the corresponding matrix of size $(M \times M)$ should be obtained as a sum of k permutation matrices. For example, consider the protograph shown in Figure 1.

Figure 1. Example of an ARJ protograph.

The corresponding base-graph matrix and the example of parity-check matrix of LDPC code with lifting size $M = 3$ are represented in (3) and (4):

$$\mathbf{B} = \begin{bmatrix} 2 & 0 & 0 & 0 & 1 \\ 3 & 1 & 1 & 1 & 0 \\ 1 & 2 & 1 & 2 & 0 \end{bmatrix}, \tag{3}$$

$$\mathbf{H} = \begin{bmatrix} 1 & 0 & 1 & 0 & 0 & 0 & 0 & 0 & 0 & 0 & 0 & 0 & 0 & 0 & 1 \\ 1 & 1 & 0 & 0 & 0 & 0 & 0 & 0 & 0 & 0 & 0 & 0 & 1 & 0 & 0 \\ 0 & 1 & 1 & 0 & 0 & 0 & 0 & 0 & 0 & 0 & 0 & 0 & 0 & 1 & 0 \\ 1 & 1 & 1 & 0 & 0 & 1 & 1 & 0 & 0 & 0 & 1 & 0 & 0 & 0 & 0 \\ 1 & 1 & 1 & 1 & 0 & 0 & 0 & 1 & 0 & 0 & 0 & 1 & 0 & 0 & 0 \\ 1 & 1 & 1 & 0 & 1 & 0 & 0 & 0 & 1 & 1 & 0 & 0 & 0 & 0 & 0 \\ 0 & 1 & 0 & 0 & 1 & 1 & 0 & 1 & 0 & 1 & 1 & 0 & 0 & 0 & 0 \\ 0 & 0 & 1 & 1 & 0 & 1 & 0 & 0 & 1 & 0 & 1 & 1 & 0 & 0 & 0 \\ 1 & 0 & 0 & 1 & 1 & 0 & 1 & 0 & 0 & 1 & 0 & 1 & 0 & 0 & 0 \end{bmatrix}. \tag{4}$$

Notice that, without lifting, the protograph shown in Figure 1 with BG matrix (3) cannot represent any code and matrix (4) is not a unique representation of BG (3). It is possible to construct the SC-LDPC code by splitting the original BG into a set of BG matrices $\mathbf{B}_i$ in such a way that

$$\mathbf{B} = \sum_{i=0}^{w} \mathbf{B}_i. \tag{5}$$

where w is the SC memory.

Then, the BG of the SC-LDPC code can be written in the form of

$$\mathbf{B}_L = \begin{bmatrix} \mathbf{B}_0 & & & & & \\ \mathbf{B}_1 & \mathbf{B}_0 & & & & \\ \vdots & \ddots & \ddots & & & \\ \mathbf{B}_w & \cdots & \mathbf{B}_1 & \mathbf{B}_0 & & \\ & \ddots & & \ddots & \ddots & \\ & & \ddots & & \ddots & \mathbf{B}_0 \\ & & & \ddots & & \mathbf{B}_1 \\ & & & & \ddots & \vdots \\ & & & & & \mathbf{B}_w \end{bmatrix}, \tag{6}$$

where L is the number of transmitted consecutive blocks (initial protographs), i.e., defining the block code of length MLb_v with the number of CNs $M(L + w)b_c$, where b_v is the number of BG VNs and b_c is the number of BG CNs. The rate of the corresponding code is

$$R_L = \frac{Lb_v - (L+w)b_c}{(L+w)b_c}. \tag{7}$$

As can be seen from the structure of the BG matrix (6), the CN degrees at both ends of the code are lower. It should be noted that CNs with lower degrees (at the ends) improve the BP decoding. This irregularity caused by the fact that w top and w bottom blocks of CNs in (6) are of lower degrees is one of the main reasons for the excellent performance of SC-LDPC codes [4]: the small-degree CNs serve as starting points for the convergence of the iterative decoding process such that a "wave" of reliable information propagates towards the middle of the codewords.

A BP decoding analysis of SC-LDPC codes shows that the performance of the iterative decoder is improved significantly by spatial coupling. In fact, the results in [4] and [5] show that asymptotically, as $L \to \infty$, the BP threshold is boosted to that of the optimal Maximum a Posteriori (MAP) decoder. Since the MAP thresholds of regular LDPC ensembles with increasing node degrees are known to converge to capacity, it follows that spatial coupling provides a new way of provably achieving capacity with low-complexity iterative BP decoding [6].

The Quasi-Cyclic LDPC (QC-LDPC) codes are of special interest due to the fact that they have efficient encoder and decoder implementations. If each $(M \times M)$ permutation matrix substituting non-zero elements in BG is a circulant, the corresponding matrix $\mathbf{H}$ defines a QC-LDPC code. In [2]-[3], the QC-LDPC codes were thoroughly studied and the effective code construction with ensemble minimum distance growing linearly with block size was proposed. This code family is called ARJ construction. An example of a BG representing ARJ construction is shown in Figure 1 [3].

The ARJ-based SC-LDPC code with memory $w = 2$ was chosen for the comparison in this paper. As it was mentioned above the Belief Propagation (BP) decoding threshold approaches capacity for all SC-LDPC codes with $L \to \infty$. Except this the ARJ-based SC-LDPC codes show better than regular code based SC-LDPC codes minimum distance growth rate [8]. That means minimum distance increases linearly with block length n and for ARJ-based SC-LDPC this increase is more than for SC-LDPC codes based on regular codes.

After simple optimization, the following partitioning of the BG (3) was chosen

$$\mathbf{B}_0 = \begin{bmatrix} 1 & 0 & 0 & 0 & 0 \\ 1 & 1 & 0 & 0 & 0 \\ 0 & 1 & 1 & 1 & 0 \end{bmatrix},$$

$$\mathbf{B}_1 = \begin{bmatrix} 1 & 0 & 0 & 0 & 0 \\ 1 & 0 & 0 & 1 & 0 \\ 0 & 1 & 0 & 0 & 0 \end{bmatrix}, \tag{8}$$

$$\mathbf{B}_2 = \begin{bmatrix} 0 & 0 & 0 & 0 & 1 \\ 1 & 0 & 1 & 0 & 0 \\ 1 & 0 & 0 & 1 & 0 \end{bmatrix}.$$

In case lifting sub-matrices are chosen to be a circulant (leading to QC code), the optimization of the lifting

permutation sub-matrices is reduced to the choice of the circulant powers. The corresponding lifting powers were optimized for lifting size $M = 8$.

B. Staircase codes

Staircase codes and braided block codes comprise the two most known representatives of the GPC [17]. Moreover, both constructions provide quite similar performance. For this reason, it was decided to limit the scope of the GPC study to staircase codes only.

Staircase codes introduced in [15] can also be considered as an example of spatially coupling principle. The staircase code construction combines ideas from recursive convolutional coding and block coding. Staircase codes are completely characterized by the relationship between successive matrices of symbols. Specifically, consider the (infinite) sequence $B_0, B_1, B_2, ...$ of $(m \times m)$ matrices B_i. For simplicity, consider each matrix B_i as a binary matrix (it can be generalized to non-binary case as well).

Block B_0 is initialized to a reference state known to the encoder–decoder pair, e.g., an $(m \times m)$ matrix of zero symbols. Furthermore, select a conventional linear block code (e.g., Hamming, Bose–Chaudhuri–Hocquenghem (BCH), RS, etc.) in systematic form to serve as the component code; this code C, is selected to have block length $2m$ symbols, of which r are parity symbols. Encoding proceeds recursively on the B_i. For each i, $m(m - r)$ information symbols (from the streaming source) are arranged into the $(m - r)$ leftmost columns of B_i; we denote this submatrix by $B_{i,L}$. Then, the entries of the rightmost r columns (this submatrix is denoted by $B_{i,R}$) are specified as follows.

1) *Form the $(m \times (2m - r))$ matrix $A = \begin{bmatrix} B_{i-1}^T & B_{i,L} \end{bmatrix}$.*

2) *The entries of $B_{i,R}$ are then computed such that each of the rows of the matrix $\begin{bmatrix} B_{i-1}^T & B_{i,L} & B_{i,R} \end{bmatrix}$ is a valid codeword of C. That is, the elements in the jth row of $B_{i,R}$ are exactly the r parity symbols that result from encoding the $2m - r$ "information" symbols in the jth row of A.*

Generally, the relationship between successive blocks in a staircase code satisfies the following relation: for any $i \geq 1$, each of the rows of the matrix $[B_{i-1}^T \ B_i]$ is a valid codeword in C. An equivalent description, from which the term "staircase codes" originates is suggested in Figure 2, in which (the concatenation of the symbols in) every row (and every column) in the "staircase" is a valid codeword of C.
The rate of a staircase code is

$$R = 1 - \frac{r}{m}, \qquad (9)$$

since encoding produces r parity symbols for each set of $m - r$ "new" information symbols.

At the end of the information sequence, termination can be used to protect the final information block. In this case, after L information blocks enter the encoder, Λ additional all-zero blocks enter the encoder. Note that the all-zero blocks are not sent over the channel, but the resulting parity bits are transmitted.
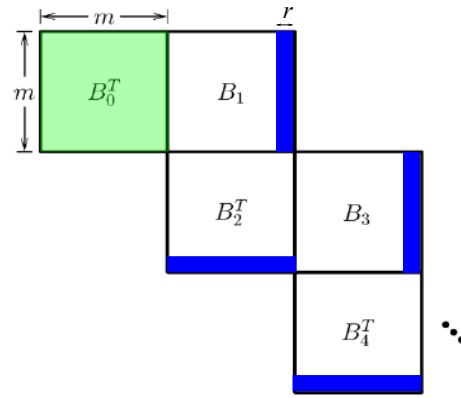

Figure 2. "Staircase" visualization of staircase codes [15].

Then, the actual rate of the staircase code, including the tail, is given by

$$R = \frac{m - r}{m + \Lambda \frac{r}{L}}. \qquad (10)$$

The staircase codes are well suited for HDD. In this case, low complexity syndrome decoder can be used for decoding a component code. Efficient, high-throughput table-lookup based methods for decoding the component codes are highlighted in [15]. On the other hand, SDD is also possible to use for a component code decoder [16].

It is easy to verify that the structure of the staircase code parity-check matrix is very similar to the structure of SC-LDPC code parity-check matrix (6):

$$\mathbf{H}_{St} = \begin{bmatrix} \mathbf{H}_2 & \mathbf{H}_1 & \mathbf{H}_0 & 0 & ... & ... & 0 & ... \\ 0 & 0 & \mathbf{H}_2 & \mathbf{H}_1 & \mathbf{H}_0 & 0 & 0 & ... \\ 0 & 0 & 0 & 0 & \mathbf{H}_2 & \mathbf{H}_1 & \mathbf{H}_0 & ... \\ \vdots & \vdots & \vdots & \vdots & 0 & 0 & \mathbf{H}_2 & \ddots \end{bmatrix}. \qquad (11)$$

The difference is that, in the staircase code parity-check matrix, the number of $(2m \times 2m)$ submatrices $\mathbf{H}_i$ is exactly 3, and each bunch of rows in (11) is shifted by the size of 2 sub-matrices. One more attractive property of the staircase codes is that the minimum distance of the staircase code is no less than d_{min}^2, where d_{min} is the minimum distance of a component code [15].

III. DECODING OF THE CONSIDERED CODES

In this study, the SC-LDPC codes were decoded with the help of SDD only. Decoding of the staircase codes was considered for both SDD and HDD.

A. Decoding of SC-LDPC codes

The convolutional structure of SC-LDPC allows to define a latency constrained decoder using a sliding window of size W. Consider the blocks of VNs of size Mb_v. Due to the convolutional structure of matrix (6) two VN blocks with indices i and j, such that $j \geq i + w + 1$, do not share any parity-check equation, i.e., VNs from these blocks cannot be

connected to the same CN. Window decoder exploits this property of the convolutional parity-check matrix of SC-LDPC code to define a decoder that deals with W received blocks such that $W \geq w + 1$. It has been shown in [7] that SC-LDPC codes decoded with a window decoder outperforms LDPC block codes under equal latency.

The most common window decoding uses the VN-centered strategy where a decoding window of size W is defined by the set of VNs for W consecutive blocks (of size Mb_v each). Some VNs on the left-hand side of the decoding window then share CNs with VNs that have already moved out of that window. CN→VN messages sent along the corresponding edges are not updated any longer, i.e., they are read-only. Similarly, some VNs on the right-hand side of the decoding window share CNs with VNs that have not yet been processed by the WD. The messages along the corresponding edges are also not updated in the current window. In terms of parity-check matrix, the sliding window decoder of size W operates on a section of WMb_c rows (CNs) and WMb_v columns (VNs) of the matrix $\mathbf{H}_L$, corresponding to W coupled blocks. Figure 3 depicts the decoding window of size 4 when assuming an SC-LDPC code with memory $w = 2$. The grey rectangles correspond to the parts of parity-check matrix not involved in the decoding process. The parts of parity-check matrix corresponding to currently (at moment t) updated VNs are marked with red. Other parts of parity-check matrix belonging to the same window are marked with blue. Performing updates on VNs in the window still requires access to messages sent along edges connected to previously decoded VNs, i.e., parts of matrix depicted by green. However, those accesses are read-only. Moving the sliding window to the next position means shifting it down by Mb_c CNs and right by Mb_v VNs.
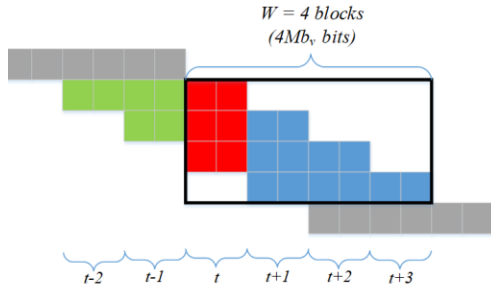

Figure 3. Parts of parity-check matrix involved in window decoding.

The window BP decoder consists of WMb_c CNs and WMb_v VNs. The decoding performance depends on the sub-block size b_v and the memory w, rather than on L. This *locality* property allows using decoder structures that are independent of L in terms of complexity, storage requirements and latency. Since the window size W is a decoder parameter, it can be varied without changing the code, providing a flexible trade-off between performance and latency [7]. In general, the storage requirements for the decoder reduces by a factor of $\frac{L}{W}$ compared to the BP decoder operating on the length of the whole codeword.

It is assumed that the window decoder uses all iterations locally inside one window position and only after fully decoding target VNs, the window is shifted to the next position. That makes it possible to unroll the iterations, which can significantly decrease the overall latency up to N_{ItMax} times (where N_{ItMax} is the maximum number of iterations), keeping the area requirements not too high. The unrolled window decoder requires CN network of $N_{ItMax}WMb_c$ CN processors, rather than $N_{ItMax}LMb_c$ CN processors in case of decoding the whole codeword.

The complexity of a decoder can be roughly estimated as follows.

Each CN input should be updated once for each layer. Considering the structure of sub-matrices (8) we can assume that each VN in window is updated on average 3 times before being used in CN processing, which translates to $3WMb_v$ additions ($120W$ additions for $M = 8, b_v = 5$) per window per iteration. On average, each CN is connected to 5 VNs, i.e., each CN processing involves on average 20 box-plus operations for SP or 20 min operations for MS (since the CN output should be generated for each of 5 connected VNs and each CN output involves $(5 - 1) = 4$ box-plus or min operations). That gives $20WMb_c = 480W$ box-plus or min operations per window per iteration. We can assume that on average $5M$ LLRs are updated at each layer, which translates to $5MWb_c = 120W$ additions per window per iteration. Then, the overall decoding complexity can be estimated as $240LN_{ItMax}W$ additions and $480LN_{ItMax}W$ box-plus or min operations for SP and MS algorithm correspondingly, where L is the number of blocks (code length is $MLb_v = 40L$), and N_{ItMax} denotes maximum number of iterations. The required memory can be estimated as $WMb_c = 24W$ elements to store CN outputs in current window.

B. Decoding of staircase codes

Staircase codes in this study were decoded both with SDD and HDD methods. In SDD, the one-sweep optimal decoding [10] was used for a component code decoding. In HDD mostly some low complexity modifications of Bounded Distance Decoding (BDD) were applied for decoding of a component code.

Similarly to the SC-LDPC code decoding, the SDD of the whole staircase code is based on the concept of windowing decoding. Consider the iterative decoding for window of length $W = 3$ for simplicity. Assuming that the target block is B_i, blocks B_{i-1}, B_i and B_{i+1} are involved in the iterations. Denote by $\mathbf{L}_j^{(ch)}$ the channel Log-Likelihood Ratios (LLRs) corresponding to $(m \times m)$ block B_j, by $\mathbf{L}_j^{(app)}$ the a posteriori probability (APP) LLRs corresponding to APPs obtained after decoding the component codes, by $\mathbf{L}_j^{(a)}$ the a priori LLRs, and by $\mathbf{L}_j^{(e)}$ the extrinsic LLR corresponding to block B_j. For window length $W = 3$ the extrinsic LLRs corresponding only to block B_i are exchanged in iterations. At first half-iteration the input for the first m symbols of the received sequence $\mathbf{y}$ is formed by LLRs chosen from $\mathbf{L}_{i-1}^{(app)}$ and the input for symbols $y_{m+1}, \dots, y_n$ is formed by the LLRs from the sum $\mathbf{L}_i^{(a)} + \mathbf{L}_i^{(ch)}$.

We assume that block B_{i-1} is already decoded, or in case B_1 is the target block, block B_0 is known a priori. At first iteration a priori LLRs are assumed to be zero, i.e., $\mathbf{L}_i^{(a)} = \mathbf{0}_{m \times m}$. After decoding of m codewords, the extrinsic LLRs are formed:

$$\mathbf{L}_i^{(e)} = \mathbf{L}_i^{(app)} - \mathbf{L}_i^{(a)}, \qquad (12)$$

and the extrinsic LLRs $\mathbf{L}_i^{(e)}$ are provided for the second half-iteration as an a priori information. At second half-iteration first m input LLRs are chosen from the sum $\mathbf{L}_i^{(a)} + \mathbf{L}_i^{(ch)}$, where $\mathbf{L}_i^{(a)}$ is substituted by the extrinsic LLRs (12) obtained at first half iteration. The input LLRs corresponding to symbols $y_{m+1}, \dots, y_n$ are chosen from the LLRs $\mathbf{L}_{i+1}^{(ch)}$. After decoding, the extrinsic LLRs are provided as an a priori LLRs for the next iteration.

Now consider the computation complexity of staircase code SDD. The number of operations (additions and multiplications) required for one-sweep decoding is half of needed for the Bahl, Cocke, Jelinek and Raviv (BCJR) algorithm and can be estimated as $O(n2^{n-k})$ per one codeword, i.e., $O(2m(W-1)n2^{n-k})$ operations per iteration per target block. The required memory corresponds to storage of one section of the trellis, i.e., 2^{n-k}. Calculation of the extrinsic information requires $2m^2(W-2)$ additions per iteration per block. Then, the overall computation complexity can be estimated as $LN_{ItMax}\big(2m^2(W-2) + O(2m(W-1)n2^{n-k})\big)$ operations, where L denotes the number of blocks and N_{ItMax} maximum number of iterations. Obviously, the overall complexity of SDD grows exponentially with $(n-k)$. Thus, only codes with the low correcting capability can be considered for a component code.

HDD imposes serious performance loss in comparison with SDD (usually around 2 dB). On the other hand, using HDD of a component code can be very attractive from the computational complexity point of view. Another argument supporting HDD is that it provides more flexibility in using different codes as a component code. As it was mentioned previously the computational complexity of the syndrome-based decoding grows exponentially with the syndrome size and therefore the choice of the codes that can be used as a component code is very limited. Of course, another possible option is to use BP algorithm for the component code decoding. However, this option also limits the choice of a component code since most part of known good codes are not suitable for BP decoding due to low girth. That limits us to use LDPC codes as component code but usually short LDPC codes provide quite low performance and in case of using longer LDPC codes as component code the decoding complexity grows fast as well. One of the most attractive features of HDD is that it is possible to use low-resolution exchange messages for iterative decoding.

The simplest iterative decoding algorithm of staircase codes is based on the bounded-distance decoding (BDD) [15]. Usually it is called iterative BDD (iBDD) algorithm or intrinsic message passing.

In [11], Extrinsic Message Passing (EMP) algorithm was proposed. It improves the iBDD performance with almost negligible decoding complexity increase.

Recently, several hybrid decoding schemes combining SDD and HDD architectures have been proposed, which provide a suitable performance-complexity tradeoff between SDD and HDD. The unifying idea of these schemes is to employ HDD as the decoding core, while exploiting some level of soft information to improve the overall decoder performance. Examples of such an approach can be found in [12] - [14].

If a linear binary code is used as a component code very simple syndrome decoding can be used for decoding of a component code. The complexity of the component code decoder in this case is defined by the complexity of a syndrome calculation, which requires $(n-k)n$ XOR operations. The drawback of this method is quite high memory requirements, which are $O(2^{n-k})$ elements. In this case, the decoding algorithm is stick to one particular code.

If BCH codes are used as a component code, it is possible to apply the algebraic decoding. In this case, the computational complexity of the algorithm can be estmated by the number of operations in Galois field $GF(2^{\log_2 n})$. The overall number of operations in Galois field (including calculation of error values that is redundant for BCH codes) can be estimated as $6nt + 9t^2$, where t is the number of correctable errors (error correcting capability of the code). In this case, the memory requirements are practically negligible since the memory is used only for storing the coefficients of polynomials of power no more than $(n-k)$.

In the same manner as in SDD, windowed decoding can be used in HDD as well. In this case, decoding of one target block requires decoding of $2m(W-1)$ codewords per iteration. If the EMP is used for HDD the only additional opeartions needed to calculate the messages is some small amount of logic operations. In case hybrid approach, e.g., like in [13] is used, the required additional complexity to calculate the messages is not negligible. For example, calculation of LLRs according to [13] requires $2m^2(W-2)$ additions per iteration per block. Then, the overall computation complexity can be estimated as $LN_{ItMax}(2m(W-1)(n-k)n)$ XOR operations and $LN_{ItMax}\big(2m^2(W-2)\big)$ additions, if syndrome decoder is used and as $LN_{ItMax}\big(2m(W-1)(6nt + 9t^2)\big)$ operations in Galois field if algebraic decoding is applied for decoding of a component code. If EMP (or any other binary message passing) is used $2m^2(W-2)$ bits is enough to store the messages. In case of hybrid approach, the required memory amount should be increased according to message resolution, e.g., for ternary message passing in [13] the memory size increases up to $4m^2(W-2)$ bits. In case the syndrome decoding is used, additional $O(2^{n-k})$ memory elements are required. In case of calculation parallelization, the amount of memory should be increased according to the number of parallel processes.

IV. COMPARISON OF THE CONSIDERED CODES

In this section, we will try to compare the considered codes taking into account how easy the code or code family can be

adapted to different code rates. We will try to compare both performance and decoding complexity of the codes with similar parameters.

A. SDD of both SC-LDPC and staircase codes

The most obvious way of adapting the code to the different code rates is to construct a mother code of low code rate and then puncture parity-check bits to obtain codes of higher rates.

For comparison the following mother codes were constructed.

SC-LDPC ARJ based mother code was constructed in line with the description in Section II with the following parameters:

- Memory size $w = 2$;
- Lifting size $M = 8$;
- Number of blocks $L = 55$;
- Code length $N_{SC-LDPC} = 2200$;
- Mother code rate $R_{SC-LDPC_{init}} = 0.38$.

Windowed SPA layered decoding with window size $W = 9$ blocks and maximum number of iterations $N_{ItMax} = 5$ was used. Floating point messages are used for message passing.

In the staircase mother code, extended $(32, 21)$ BCH code capable of correcting 2 errors was used as a component code $(m = 16, r = 11)$. The staircase mother code parameters are:

- Number of blocks $L = 8$;
- Number of terminating blocks $\Lambda = 0$;
- Code length $N_{St} = 2048$;
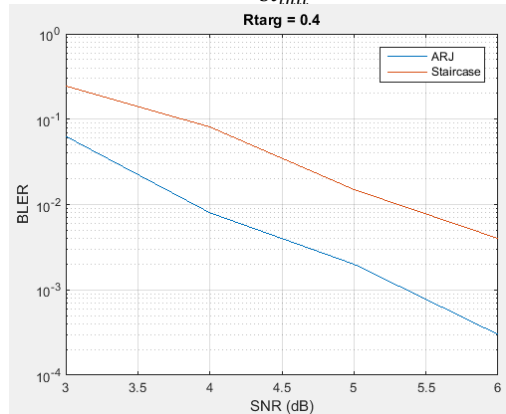- Mother code rate $R_{St_{init}} = 0.31$.

Figure 4. Performance comparison of ARJ based SC-LDPC ($N_{SC-LDPC} = 2200$) and staircase code ($N_{St} = 2048$) at Rtarg = 0.4. SDD.

The staircase code was decoded with the help of the SDD described in Section III.B with window size $W = 3$ blocks and maximum number of iterations $N_{ItMax} = 5$. The syndrome based one-sweep decoding was applied for decoding of a component code. Floating point messages are used for message passing.

Simulation results for different code rates R_{targ} are represented in Figure 4, 5 and 6.

As can be seen from Figure 4, 5 and 6, with target code rate $R_{targ} = 0.4$, the SC-LDPC code outperforms the staircase code by more than 1 dB. However, with increasing

target code rate, this performance gap decreases and at $R_{targ} = 0.7$ it is negligible. This can be explained by the fact that the initial mother code rate of the ARJ-based is higher, but puncturing deteriorates its performance faster than the performance of the staircase code.
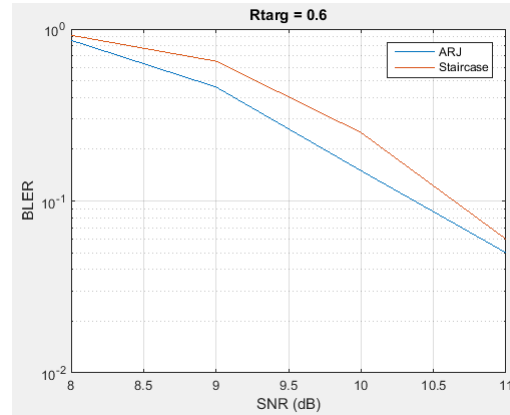

Figure 5. Performance comparison of ARJ-based SC-LDPC ($N_{SC-LDPC} = 2200$) and staircase code ($N_{St} = 2048$) at Rtarg = 0.6. SDD.
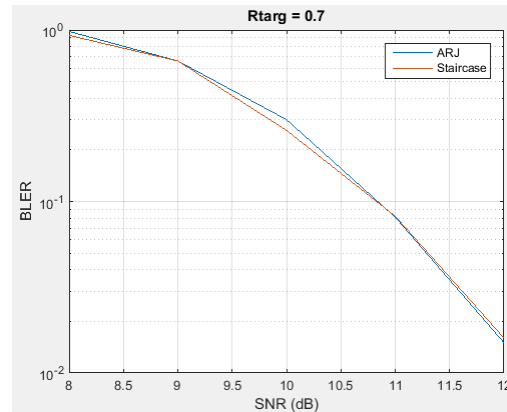

Figure 6. Performance comparison of ARJ-based SC-LDPC ($N_{SC-LDPC} = 2200$) and staircase code ($N_{St} = 2048$) at Rtarg = 0.7. SDD.

Comparing the decoding complexity of used decoders according to estimates in Section III.A and Section III.B we can observe that the complexity of the staircase decoder is about 3 - 4 times higher than the complexity of the SC-LDPC decoder (depending on how to estimate the complexity of the box-plus operation).

Taking into account the lower computational complexity and better performance of the ARJ-based SC-LDPC code, it would be the obvious choice for SDD. On the other hand, the drawback of this code family is the serious performance degradation with target rate increase. Most probably with some optimization efforts it would be possible to find some specific puncturing patterns that can provide not so fast performance degradation but it will take time to find optimal distribution of punctured bits between the sub-matrices of the parity-check matrix.

B. HDD for staircase codes

As it was mentioned in Section A, the complexity of SDD for staircase codes is too high and the performance is inferior to the performance of the ARJ-based SC-LDPC code at low code rates. However, the performance of staircase codes does not drop as fast as the performance of the SC-LDPC codes with the code rate increase.

Since our goal is to consider the codes that can provide high throughput, it might be interesting to consider the possibility of using HDD. As it was discussed in Section III.B, the staircase codes are especially attractive for the HDD since some good codes allowing low-complexity algebraic decoding can be used as a component code. Moreover, the performance drop due to applying HDD rather than SDD can be partly compensated by usage of more powerful codes, which are not possible to use in SDD due to prohibitively high decoding complexity.

For example, it is possible to consider RS codes as component codes. Except the good performance one of the attractive properties of the RS codes is that they belong to the class of Maximum Distance Separable (MDS) codes for which any k symbols of a codeword, where k is the number of information symbols, forms the information sequence. Due to this property all puncturing patterns for RS codes are equally good and there is no need in designing special puncturing patterns when adapting the mother code for the target code rate.

In this section, we consider the comparison of longer codes. We again apply SDD for decoding of the SC-LDPC code, but of lower complexity. We consider Min-Sum (MS) algorithm rather than Sum-Product Algorithm (SPA) and decrease the exchanged message resolution. High resolution of the exchanged messages can hinder achieving high throughput since it will require a lot of additional wiring in comparison with the low resolution message passing leading to serious limitation in possible parallelizing of computations. Thus, the binary message passing is especially attractive for high throughput decoders. In our simulations, we decrease the message resolution to 3 bits.

The parameters of the SC-LDPC ARJ-based mother code used in the simulations are as follows:

- Memory size $w = 2$;
- Lifting size $M = 8$;
- Number of blocks $L = 510$;
- Code length $N_{SC-LDPC} = 20400$;
- Mother code rate $R_{SC-LDPC_{init}} = 0.398$.

Windowed MS layered decoding with window size $W = 18$ blocks and maximum number of iterations $N_{ItMax} = 5$ was used. 3 bits messages are used for message passing.

In the staircase mother code, extended $(32, 23)$ RS code over the $GF(2^5)$ capable of correcting 4 errors was used as a component code, i.e., the code length in bits is $32 \cdot 5 = 160$ ($m = 80 \ bits, \ r = 45 \ bits$). The staircase mother code parameters are:

- Number of blocks $L = 3$;
- Number of terminating blocks $\Lambda = 1$;
- Code length $N_{St} = 22800$;
- Mother code rate $R_{St_{init}} = 0.368$.

The staircase code was decoded with the help of the binary message passing with window size $W = 3$ blocks and maximum number of iterations $N_{ItMax} = 5$, the algebraic decoding of the component RS code was used. Notice, that despite the exchanged messages have 5 bit resolution, this is 5 bit message per $GF(2^5)$ symbol, i.e., per 5 bits. Thus, we can consider it as a binary message passing.

Performance comparison of the ARJ-based SC-LDPC code (MS decoding, 3 bit message) and $(32, 23)$-RS-based staircase code ($m = 80 \ bits$, 1 bit message) is shown in Figures 7, 8 and 9.
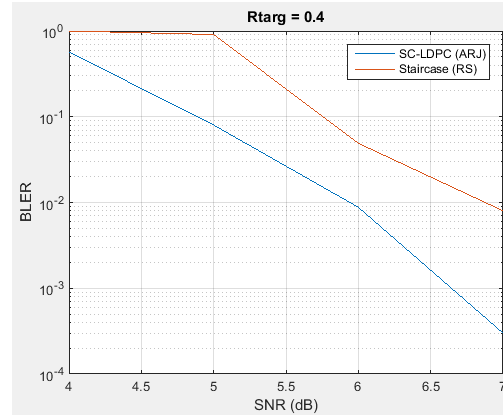

Figure 7. Performance comparison of ARJ based SC-LDPC ($N_{SC-LDPC} = 20400$) and RS-based staircase code ($N_{St} = 22800$) at Rtarg = 0.4. MS decoder for SC-LDPC, HDD for staircase code.
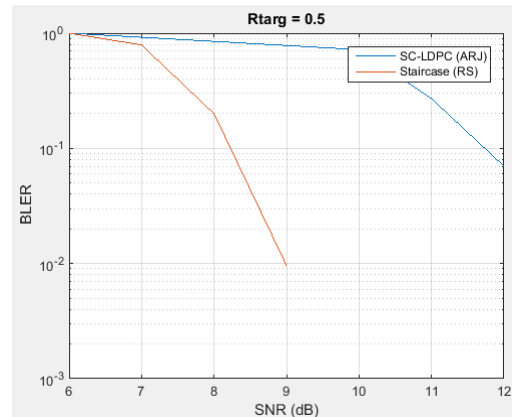
Figure 8. Performance comparison of ARJ based SC-LDPC ($N_{SC-LDPC} = 20400$) and RS-based staircase code ($N_{St} = 22800$) at Rtarg = 0.5. MS decoder for SC-LDPC, HDD for staircase code.

As can be seen from Figures 7, 8 and 9, the performance of the ARJ based SC-LDPC code deteriorates much faster with the target rate increase than the performance of the RS-based staircase code. At the same time, the performance of the RS-based staircase code changes quite smoothly with code rate increase.

Comparison of the decoding complexity depends on how to estimate the computational complexity of min operation and the operation in Galois field. Assuming that the computational complexity of the min operation is equal to

addition complexity, and the operation in Galois field has the same complexity (addition in Galois field is equivalent to XOR operation and multiplication is equivalent to addition on modulo $(n-1)$, where n is the RS code length, or both operations can be implemented with Look-Up Table (LUT)), we can estimate that the decoding complexity of the ARJ based SC-LDPC code is $7-8$ times greater than that of RS-based staircase code.

Figure 9. Performance comparison of ARJ based SC-LDPC ($N_{SC-LDPC} = 20400$) and RS-based staircase code ($N_{St} = 22800$) at Rtarg = 0.7. MS decoder for SC-LDPC, HDD for staircase code.
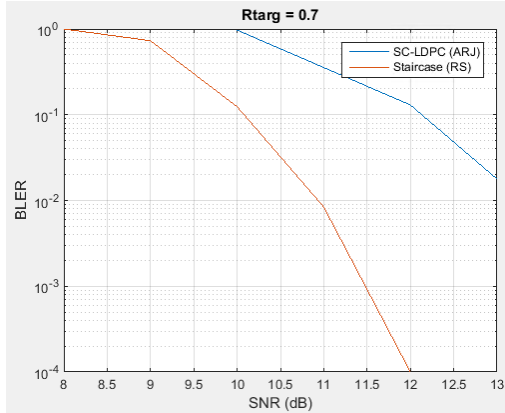
Moreover, with current parameters the amount of memory needed for storing the exchanged messages in window for ARJ based SC-LDPC code is about 200 times more than for the RS-based staircase code if the messages in BP decoder are stored in $(b_c \cdot M \cdot W \times b_v \cdot M \cdot W)$ matrix. More realistic is the case when each message simply consists of value and address. The number of messages in windowed MS decoding of SC-LDPC code can be estimated as $5b_c \cdot M \cdot W = 2160$. Assuming that there are $b_v \cdot M \cdot W = 720$ VNs in window, each CN→VN message comprises 3 bits bearing the value and 10 bits address. That gives $2160 \cdot 13 = 28080$ bits, which 4.3 times more than 6400 bits needed for messages in staircase decoder with window size 3.

One obvious drawback of the RS-based staircase codes is less flexibility with the choice of the code length since it should be a multiple of m^2. This value depends on the choice of the RS code. However, here some optimization is also possible. For example, for Galois field $GF(2^p)$ if p is not a prime the field element can be represented differently (e.g. as a $(1 \times p)$ vector or as a $(q_1 \times q_2)$ matrix, where $q_1 \cdot q_2 = p$). Then, one representation leads to $m = p2^{p-1}$ and another to $m = q_2 2^{p-1}$. In first case, $p2^{p-1}$ RS codes should be decoded at each half-iteration for each block. The second representation leads to necessity to decode $\frac{q_2 2^{p-1}}{q_1}$ codes. Of course, the performance in case of second representation should be less than in first case but it could worth of considering. An example of staircase codes based on different representation of $GF(2^4)$ symbol is shown in Figure 10.

Two representation of $GF(2^4)$ symbol ((2×2) and (1×4)) leads to the staircase codes with different block size and therefore different code length. Both codes in Figure 10

comprise 4 information blocks and 1 terminating block ($\Lambda = 1$). Obviously both codes have the same original rate $R = 0.3243$. Representation (2×2) gives the block size $m = 16$ (8 RS codes must be decoded in block), which leads to the original code length $N_{St} = 1184$, and representation (1×4) gives the block size $m = 32$ (32 RS codes must be decoded in block) leading to the original code length $N_{St} = 4736$. As can be seen from the performance curves in Figure 10, the behavior of both codes is quite similar with changing target code rate.
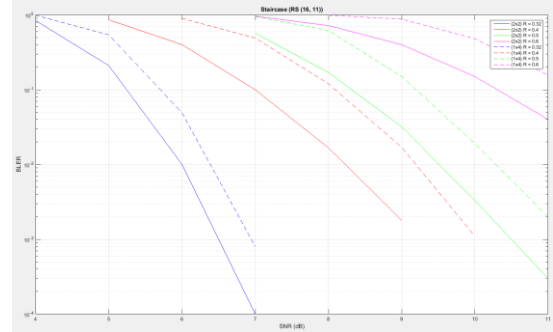

Figure 10. Performance of staircase code based on (16, 11) RS code with different representation of GF(2^4) symbol. (2×2) and (1×4).

In case performance provided by the HDD of RS codes is not enough, two other options can be considered. One of them is to apply soft decoding of RS codes based on Guruswami-Sudan (GS) list decoding [18]. Another is to consider LDPC codes as a component code. On the other hand, both options lead to severe complexity increase. For example, even applying Nielsen interpolation to GS, overall complexity of the list decoding is $O\left(n^2 \left(\frac{n}{k}\right)^{1/2} r^5\right)$ [19], which again narrows the choice of a component code.

V. CONCLUSIONS

The performance and complexity comparison of the ARJ based SC-LDPC codes and staircase codes shows that SDD SC-LDPC codes provide better performance and lower complexity than the staircase codes. However, the performance of SC-LDPC codes deteriorates very fast with code rate increase.

The usage of HDD together with the powerful RS codes brings a benefit of significant complexity decrease with an affordable performance loss. Moreover, the performance of the RS-based staircase codes changes quite smoothly with the code rate increase. One more benefit of HDD of the RS-based staircase codes is the possibility of usage of binary message passing, which decreases significantly the amount of data exchange between the nodes. The latter property is especially important for reaching a high throughput.

Therefore, the HDD of the RS-based staircase code can be considered as a good option for high-throughput decoding. In case higher performance will be needed, one of the interesting directions could be considered: the usage of LDPC codes as component codes in staircase code and BP decoding of a component code.

REFERENCES

[1] A. Jimenez Felstrom and K. Zigangirov, "Time-varying periodic convolutional codes with low-density parity-check matrix," IEEE Trans. Inf. Theory, vol. 45, pp. 2181 – 2191, September 1999.

[2] D. Divsalar, C. Jones, S. Dolinar, and J. Thorpe, "Protograph Based LDPC Codes with Minimum Distance Linearly Growing with Block Size," IEEE Globecom 2005, pp. 1152 – 1156, 2005.

[3] D. Divsalar, S. Dolinar, C. Jones, and K. Andrews, "Capacity-approaching protograph codes," IEEE Journal on Select Areas in Communications, vol. 27, no. 6, pp. 876 – 888, 2009.

[4] M. Lentmaier, A. Sridharan, D. Costello, and K. Zigangirov, "Iterative decoding threshold analysis for LDPC convolutional codes," IEEE Trans. Inf. Theory, vol. 56, pp. 5274 –5289, Oct. 2010.

[5] S. Kudekar, T. Richardson, and R. Urbanke, "Threshold saturation via spatial coupling: Why convolutional LDPC ensembles perform so well over the BEC," IEEE Trans. Inf. Theory, vol. 57, pp. 803–834, Feb. 2011.

[6] M. Lentmaier, I. Andriyanova, N. Hassan, and G. Fettweis, "Spatial Coupling - A way to Improve the Performance and Robustness of Iterative Decoding," Proc. European Conf. Networks and Communications (EuCNC), pp. 1 – 4, 2015.

[7] N. Hassan, M. Lentmaier, and G. Fettweis, "Comparison of LDPC block and LDPC convolutional codes based on their decoding latency," in Proc. Int. Symp. on Turbo Codes & Iterative Inf. Proc., pp. 225 – 229, Aug. 2012.

[8] D. Mitchell, M. Lentmaier, and D. Costello, "Spatially coupled LDPC codes constructed from protographs," IEEE Trans. Inf. Theory , vol. 61, no. 9, pp. 4866 – 4889, 2015.

[9] K. Klaiber, S. Cammerer, L. Schmalen, and S. ten Brink, "Avoiding Burst-like Error Patterns in Windowed Decoding of Spatially Coupled LDPC," Proc. IEEE 10th International Symposium on Turbo Codes & Iterative Information Processing (ISTC), pp. 1 – 5, 2018.

[10] T. Johansson and K. Sh. Zigangirov, "A simple one-sweep algorithm for optimal APP symbol decoding of linear block codes," IEEE Trans. Inf. Theory, vol. 44, no. 7, pp. 3124–3129, Nov. 1998.

[11] Y. Jian, H. Pfister, K. Narayanan, R. Rao, and R. Mazahreh, "Iterative Hard Decision Decoding of Braided BCH Codes for High Speed Optical Communication," Proc. GLOBECOM, pp. 2376 – 2381, 2013.

[12] A. Sheikh, A. Graell i Amat, G. Liva, C. Häger, and H. D. Pfister, "On low-complexity decoding of product codes for high-throughput fiber-optic systems," in Proc. IEEE Int. Symp. on Turbo Codes & Iterative Inf. Proc. (ISTC), Hong Kong, pp. 1 – 5, Dec. 2018.

[13] A. Sheikh, A. Graell i Amat, G. Liva, and A. Alvarado, "Refined reliability combining for binary message passing decoding of product codes," arXiv, 2020. [Online]. Available:https://arxiv.org/abs/2006.00070, pp. 1 – 5, 2020.

[14] A. Sheikh, A. Graell i Amat, G. Liva, and A. Alvarado, "Novel High-Throughput Decoding Algorithms for Product and Staircase Codes based on Error-and- Erasure Decoding," arXiv, 2020, [Online]. Available: https://arxiv.org/abs/2008.02181, pp. 1 – 12, 2020.

[15] B. P. Smith, A. Farhood, A. Hunt, F. R. Kschischang, and J. Lodge, "Staircase codes: FEC for 100 Gb/s OTN," IEEE/OSA J. Lightw. Technol., vol. 30, no. 1, pp. 110–117, Jan. 2012.

[16] X. Dou, M. Zhu, J. Zhang, and B. Bai, "Soft-Decision Based Sliding-Window Decoding of Staircase Codes," IEEE 10th International Symposium on Turbo Codes & Iterative Information Processing, pp. 1 – 5, 2018.

[17] C. Häger, H. D. Pfister, A. Graell i Amat, and F. Brännström, "Density Evolution for Deterministic Generalized Product Codes on the Binary Erasure Channel at High Rates," IEEE Trans. Inf. Theory, vol. 63, no. 7, pp. 4357 – 4378, 2017.

[18] V. Guruswami and M. Sudan, "Improved Decoding of Reed-Solomon Codes and Algebraic Geometry Codes," IEEE Trans. Inform. Theory, vol. 45, no. 6, pp. 1757 – 1767, 1999.

[19] G. Kabatiansky, E. Krouk, and S. Semenov, "Error Correcting Coding and Security for Data Networks," Wiley, 2005.

A Machine Learning Approach for Resource Allocation in Wireless Industrial Environments

Idayat O. Sanusi and Karim M. Nasr

Faculty of Engineering and Science, University of Greenwich,
Kent, ME4 4TB, United Kingdom
{i.o.sanusi, k.m.nasr}@gre.ac.uk

Abstract— **In this paper, we present a machine learning technique for channel selection in a Device to Device (D2D)-enabled cellular network targeting a wireless industrial environment. The presented Base Station Assisted (BSA) reinforcement learning technique uses a distributed local Q-table for the agents (users), to prevent global information gathering within the cellular network. A stateless Q-learning approach is adopted to reduce the complexity of learning and the dimension of the Q-table. After the training of the D2D agents, the Q-tables of the D2D users are uploaded to the base station for resource allocation to be implemented centrally. Simulations results show that the presented technique provides a Radio Resource Management (RRM) solution with a good Quality of Service (QoS) performance compared to other conventional approaches.**

Keywords— 5G and beyond networks; Radio Resource Management; Distributed Algorithms; Device-to-Device Communication; Reinforcement Learning.

I. Introduction

Device-to-Device communication (D2D) is considered as a promising solution for ultra-reliable low-latency use cases because of associated advantages in terms of reduced latency, improved reliability and throughput. The integration of D2D into future industrial wireless networks and smart manufacturing facilitates the creation of massive machine-type connections [1]. Machine-Type Communication (MTC) is expected to support large numbers of smart devices, predominantly with small data volume requirements, which aggregates into a massive amount of data from parallel transmissions of a large number of devices. Achieving ultra-high reliability and ultra-low latency pose challenges in terms of bandwidth requirements. Yilmaz et al. [2] studied the transmission bandwidth needed to enable Ultra-Reliable Low-Latency Communication (URLLC) for factory automation and found that the system bandwidth depends on the number of connected pieces of user equipment and the behaviour of their traffic. The scarcity of radio resources and the limitations on the available system bandwidth makes spectrum sharing a necessity for D2D implementation of MTC for factory automation [3]. RRM schemes need to be efficiently designed for interference management and coordination while guaranteeing tight URLLC demands.

Channel reuse among active devices in the same cells will generate interference which degrades system performance. Interference management is crucial to ensure efficient utilisation of available spectrum resources which is also particularly challenging for D2D deployments in underlay cellular networks.

The two major approaches to Radio Resource Management (RRM) are based on centralised and distributed methods. The centralised scheme requires global information gathering by base stations which often results in a high signalling overhead and increased complexity which tend to increase with the number of users, thus making it impractical. The distributed approach does not need a central entity; resource allocation is implemented by users therefore reducing the amount of information gathering and processing by base stations. However, a distributed RRM algorithm may also increase signalling overheads due to the high amount of information interchange among devices [4].

Reinforcement Learning (RL) has recently gained a lot of attention because of its suitability for the decision-making process where there is unknown or partial channel information. RL has been widely studied for intelligent power and spectrum allocations for D2D communication in cellular networks. Asheralieva and Miyanga [5] formulated the resource allocation problem as a non-cooperative game model among D2D users and a mixed strategy Nash Equilibrium was obtained. However, the Quality of Experience (QoS) metrics of cellular users sharing channel resources with D2D links were not taken into account in the reward model. A multi-agent actor-critic structure is proposed in [6] which involves interactions between users and centralised sharing of all historical information. This leads to an increase in signalling overheads and information exchange. In [5]-[8], the reward function captured the QoS metric of the cellular users in a centralised Q-learning approach, which leads to increased signalling overheads as well.

In this paper, we present a semi-distributed reinforcement learning scheme for D2D resource allocation in a cellular network in an industrial setting. After the decentralised training of the agents, their Q-tables uploaded are forwarded to the base station for a centralised resource allocation. The reward function is modeled in such a way that there is no information exchange related to other agents' action or reward. To address the problem of the 'curse of dimensionality' associated with Q-learning, a stateless Q-learning is adopted to reduce the dimension of the Q-table, nonetheless capturing the QoS demands of the D2D users.

The paper is organised as follows: The problem formulation and system model are presented in Section II. In Section III, a stateless reinforcement learning algorithm for base station-assisted resource allocation is presented. Section IV presents some results and discussions of the simulation scenarios considered. Conclusions and directions for future work are summarised in Section V.

II. SYSTEM MODEL

We consider D2D and cellular users coexisting within a cellular network for uplink spectrum-sharing. There are N Cellular User Equipment (CUEs) represented by a set C and M D2D User Equipment (DUEs) denoted by a set D randomly deployed within the coverage of the base station (BS) in a single cell system. The cellular users have strict performance requirements in the form of minimum Signal to Interference plus Noise Ratio (SINR) values to guarantee their throughput. The D2D links also have minimum SINR thresholds to guarantee their throughput demands, in addition, to the reliability and delay constraints. We assume that each CUE has been pre-allocated a resource block. The transmit power of the CUEs and DUEs are denoted by P_{c_i} and P_{d_j}, respectively. We denote $g_{c,B}$, $g_{d_T,B}$, g_{d_T,d_R} and g_{c,d_R} as the channel gains from the CUE c_i to the BS, the interference link from the DUE transmitter d_T to the BS, the D2D link from the DUE transmitter d_T to the receiver d_R and the interference link form the CUE transmitter to the DUE receiver d_R, respectively.

The instantaneous received signal-to-interference-plus-noise-ratio (SINR) at the BS from ith CUE and jth DUE over ith sub-channel at time slot t is given as:

$$\Gamma_{c_i}(t) = \frac{P_{c_i} g_{c,B}(t)}{\sigma^2 + \sum_{d_j \in D} \lambda_j^i(t) P_{d_j} g_{d_T,B}(t)} \qquad (1)$$

$$\Gamma_{d_j}(t) = \frac{P_{d_j} g_{d_T,d_R}(t)}{\sigma^2 + \sum_{c_i \in C} \lambda_j^i(t) P_{c_i} g_{c,d_R}(t)} \qquad (2)$$

$\lambda_j^i \in \{0,1\}$ denotes the binary resource reuse indicator, $\lambda_j^i = 1$ implying jth DUE selects ith CUE sub-channel at time slot t and $\lambda_j^i(t) = 0$ otherwise.

The data rates of the ith CUE and jth DUE is at time slot t are given by:

$$\text{T}_{c_i}(t) = W_i \log_2 \left(1 + \Gamma_{c_i}(t)\right) \qquad (3)$$

$$\text{T}_{d_j}(t) = W_i \log_2 \left(1 + \Gamma_{d_j}(t)\right) \qquad (4)$$

where W_i is the bandwidth of each resource block. The variance of the additive white Gaussian noise (AWGN) is denoted by σ^2. The resource allocation problem for D2D communication in cellular network is NP hard and cannot be solved directly and often requires global information gathering which increases complexity. The channel gains for links q to r can be expressed as follows:

$$g_{q,r} = G_r \gamma_{q,r} \chi_{q,r} L_{q,r}^{-\alpha_r} \qquad (5)$$

where G_r is the pathloss constant, $\gamma_{q,r}$ is the small-scale fading gain due to multipath propagation and assumed to have an exponential distribution with unit mean. The large-scale fading comprises pathloss with exponent α_r and shadowing which has a slow fading gain $\chi_{q,r}$ with a log-normal distribution. $L_{q,r}$ is the distance from terminal q to terminal r [9]. The channel gain from D2D link d_j of transmitter d_T to the receiver d_R is g_{d_T,d_R}, the channel gain of the interference link from d_T to the base station is $g_{d_T,B}$ and from CUE c_i to DUE d_j receiver is h_{c,d_R} and $h_{c,B}$, is the channel gain from CUE c_i to the base station BS. The channel gain g_{d_T,d_R} and g_{c,d_R} can be estimated at the DUE

receiver, d_R and made available at its transmitter, d_T instantaneously [10]. Similarly, $g_{c,B}$ and $g_{d_T,B}$ can be obtained at BS through local information since uplink transmission is considered. The reliability of the DUE $d_j \in D$, $\xi_{d_j}(t)$, is defined as the probability of packet delay exceeding a predefined delay bound, $l_{d_j,\max}$, for channel i at slot t is less than a threshold [11]. Only the transmission delay is considered in this work. The objective of the system is to maximise the total throughput, T_R, of paired CUE and DUEs while satisfying the QoS demands.

$$\underset{\lambda_j^i}{\text{Max}} \, T_R = W_i(\lambda_j^i(\sum_{c_i \in C} \log_2\left(1 + \Gamma_{c_i}\right) + \sum_{d_j \in D} \log_2(1 + \Gamma_{d_j}))) \qquad (6)$$

subject to:

$$\lambda_j^i \Gamma_{c_i} - \Gamma_{c_i,\min} \geq 0 \qquad \forall c_i \in C \qquad (6a)$$

$$\text{Pr}\left(l_{d_j} > l_{d_j,\max}\right) < 1 - \xi_{d_j}^* \quad \forall \, d_j \in D \qquad (6b)$$

$$\sum_{c_i \in C} \lambda_j^i \leq 1 \qquad \forall \, d_j \in D \qquad (6c)$$

$$\sum_{d_j \in D} \lambda_j^i \leq 1 \qquad \forall \, c_i \in C \qquad (6d)$$

The minimum CUE SINR, $\Gamma_{c_i,\min}$, to guarantee the throughput requirement of the CUEs is defined in constraint (6a). Constraint (6b) takes into account reliability and delay, where l_{d_j} is the packet delay constraint for packet transmission of DUE d_j. The expression captures the fact that the end-to-end delay should be less than $l_{d_j,\max}$ with a probability of at least $1 - \xi_{d_j}^*$. Constraints (6c) and (6d) are channel association criteria. The reliability of the DUE links in (6c) is evaluated using an empirical estimation of number of packets transmitted similar to [11], from d_T to d_R whose delay is within the budget $l_{d_j,\max}$ over the total number of packets sent to d_R at time slot t i.e.,

$$\xi_{d_j}(t) = 1 - \text{Pr}\left(l_{d_j} > l_{d_j,\max}\right) \approx 1 - \frac{L_{d_j}(t)}{B_{d_j}(t)} \cong \frac{L'_{d_j}(t)}{B_{d_j}(t)} \quad (7)$$

where $L_{d_j}(t)$ is the number of packets for which $l_{d_j} > l_{d_j,\max}$ and $L'_{d_j}(t)$ is the number of packets transmitted with $l_{d_j} \leq l_{d_j,\max}$ (or number of packet delivered within the delay bound). $B_{d_j}(t)$ is total packet transmitted by DUE d_j at time slot t. Reliability can also be measured in terms of the outage probability, which is the probability that the measured SINR is lower than a minimum is less than a predefined threshold. The closed expression of the outage probability of jth DUE conditioned on the selected ith channel at time slot t is given below [12].

$$p_R(t) = \text{Pr}\left(\Gamma_{d_j} \leq \Gamma_{d_j,\min}\right)$$

$$= 1 - \frac{P_{d_j} g_{d_T,d_R} \exp\left(-\frac{\Gamma_{d_j,\min} \sigma^2}{P_{d_j} g_{d_T,d_R}}\right)}{P_{d_j} g_{d_T,d_R} + \Gamma_{d_j,\min} P_{c_i} g_{c,,d_R}} \leq p_{R_0} \qquad (8)$$

where $p_R(t)$ is the measured outage probability of DUE d_j at time slot t and p_{R_0} is the maximum tolerable outage

probability of d_j. The reliability of the DUE in terms of outage probability is expressed as:

$$\xi_{d_j}(t) = 1 - p_R(t) \qquad (9)$$

Transmission delay is given as the ratio of packet size transmitted within delay bound to transmission rate [13]. From (7), (8) and (9) the transmission of jth DUE on the ith RB is formulated as:

$$l_{d_j}(t) = \frac{L'_{d_j}(t)}{W_i \log_2(1 + \Gamma_{d_j})} \qquad (10)$$

The resource allocation problem for D2D communication in a cellular network is complex and a direct solution is not feasible. We present next a base station-assisted resource allocation scheme which adopts a semi-distributive RRM approach.

III. STATELESS REINFORCEMENT LEARNING FOR BASE STATION-ASSISTED RESOURCE ALLOCATION

The goal of the agents is to maximise the throughput in a D2D-enabled cellular network. At each time slot t, a DUE, observes a state s^t and takes an action a^t from the action space, (i.e., select an RB k_i), according to the policy π. Q-learning enables an agent to determine the optimal strategy that maximises its long term expected cumulative reward [14]. The Q-value is updated as follows:

$$Q^{t+1} =$$
$$\begin{cases} Q^t(s^t, a^t) + \sigma \left[r^t + \eta \max_a Q^t(s^{t+1}, a^{t+1}) - Q^t(s^t, a^t) \right] \\ \qquad \text{if } s = s^t, \ a = a^t \\ Q^t(s^t, a^t), \ \text{otherwise} \end{cases} \qquad (11)$$

where $\sigma \in [0,1]$ is the learning rate. With $\sigma = 0$, the Q-values are never updated, hence no learning has taken place; setting σ to a high value such as means that learning can occur quickly and $0 \le \eta \le 1$ is the discount factor used to balance immediate and future reward [14].

The state-action dimension is reduced by adopting a stateless learning approach. For the considered scenario, any action $a_i \in A$ taken by an agent will result in the end of an episode i.e., states 0 and 1 are terminal states, where $S_{d_j}^i(t) = 1$ is the goal state of the DUEs. Therefore, the learning environment can be modelled entirely using a stateless Q-learning i.e., action-reward only since the state transition is not required. An agent can choose its action based solely on its Q-value and the updated Q-value of the chosen action is based on the current Q-value and the immediate reward from selecting that action. The update function in (11) is re-formulated as follows:

$$Q^{t+1}(a^t) = \begin{cases} Q^t(a^t) + \sigma[r(a^t) - Q^t(a^t)], \text{if } a = a^t \\ \qquad Q^t(a^t), \qquad \text{otherwise} \end{cases} \qquad (12)$$

where $r(a^t)$ is the immediate reward of selecting a. In contrast to the standard Q-value update function in (11), it can be seen in (12) that not only the state-action formation

(s, a) is not necessary, but also the information of the next state s^{t+1} is not required because the actions lead to a terminal state. Therefore, the Q-table is defined in terms of the actions only and updated using the immediate reward. This results in $1 \times |N|$ dimension Q-table for jth DUE. This method reduces the learning complexity and the Q-table dimension.

The traditional cellular users in the network need to be protected from the interference caused by the DUEs for their minimum SINR to be satisfied. This may be achieved by integrating the SINR of the CUE, Γ_{c_i} in the state space or reward function modelling. This way, the DUEs can obtain the information from BS at time slot t as in [15]-[17]; hence, the DUEs get a reward if the CUE SINR $\Gamma_{c_i} \ge \Gamma_{c_i,\min}$, on the and a penalty otherwise. Rather than the BS exchange the measured CUE SINR, Γ_{c_i}, with the DUEs for every action a^t taken at each time slot, we adopt a scheme in which the BS keeps a look-up table of the ith CUE based on the actions on the DUEs.

BSA Reinforcement Learning Algorithm

1: Initialise the action-value function for the DUEs
$\qquad \left[Q_{d_j}(a) = 0 | Q_{d_j}(a) \equiv Q_{d_j}^i(a^t), i = 1,2,\dots,N \right] \forall d_j \in D$

2: Initialise the action-value function for the BS for the actions of the jth DUE on the ith RB
$\qquad \left[Q_{c_i}(a) = 0 | Q_{c_i}(a) \equiv Q_{c_i}^j(a^t), j = 1,2,\dots,M \right] \quad \forall c_i \in C$

3:    **for** $d_j \in D \ 1 \le j \le M$ **do**

4:      **while** not converge **do**

5:        generate a random number $x \in \{0,1\}$

6:        **if** $x < \varepsilon$ **then**

7:          Select action a_i^t randomly

8:        **else**

9:          Select action $a_i^t = \arg\max_{a \in A} Q_{d_j}(a^t)$

10:        **end**

11:       Evaluate ξ_{d_j}, Γ_{d_j} and l_{d_j} of $d_j \in D$ for the action a^t

12:       Measure the SINR, ξ_{c_i}, of CUE $c_i \in C$ for the action a^t taken by $d_j \in D$

13:        Observe immediate reward of $d_j \in D$ and $c_i \in C$,

14:       Update action-value for action of $d_j \in D$ on the ith RB $Q_{d_j}^i(a) = Q_{d_j}^i(a) + \sigma \left[r_{d_j}(a^t) + Q_{d_j}^i(a) \right]$

15:       Update action-value for $c_i \in C$ for action a^t of jth DUE $Q_{c_i}^j(a) = Q_{c_i}^j(a) + \sigma[r_{c_i}(a^t) + Q_{c_i}^j(a)]$

16:      **end while**

17:    **end for**

18: Load $Q_{d_j}(a)$ to the BS $\qquad \forall d_j \in D$

19: **for** $d_j \in D \ 1 \le j \le M$ **do**

20:     Obtain $Q(a) = \left\{ Q_{d_j}^i(a), Q_{c_i}^j(a) \right\} \ i = 1,2,\dots,N$

21:     $\bar{Q}(a) \subseteq Q(a) | \left\{ Q_{d_j}^i(a), Q_{c_i}^j(a) \right\} \in \mathbb{R}^+$, where $\mathbb{R}^+$ positive real number

22:     $Q_{\text{TOT}} = Q_{d_j}^i(a) + Q_{c_i}^j(a) \qquad \forall q \in \bar{Q}(a)$

23: **end for**

24: Set up a list for unmatched DUE $D_u = \{ d_j : \forall d_j \in D_u \}$

25: **while** $D_u \ne \emptyset$ **do**

26:     Rank D_u in increasing order of $|0 \ \bar{Q}(a)|$

27:     Start DUE $d_j \in D_u : \bar{Q}(a) \ne \emptyset$ with the least $|\bar{Q}(a)|$

28:     $c_i^* = \max_{r_i \in R} Q_{\text{TOT}}$

29:     $D_u = D_u - d_j$

30:     $\bar{Q}(a) = \bar{Q}(a) \backslash c_i^* \qquad \forall d_{j'} \in D_u | j' \ne j$

31: **end while**

There are a number of methods to select an action based on the current evaluation of the Q-value at every time slot t using a policy denoted by $p_{d_j}^t$. These methods are used to balance exploration and exploitation [18]. Epsilon greedy (ε-greedy) is one of the methods of choosing an optimal Q-value.

The reward function is modelled such that it relies only on local observations and can be implemented in a distributive manner. The rewards of the jth DUE and ith CUE for taking an action a_i^t is expressed in terms of the achievable throughput using the Shannon capacity formula. Therefore, the reward is directly related to the objective function of the optimisation problem. The following is a summary of the Base Station Assisted (BSA) Reinforcement Learning Algorithm:

The jth DUE only gets a reward when all state variables are 1 (i.e., the minimum QoS demands are met) while ith CUE gets a reward if its minimum SINR is satisfied at each time slot for the action taken by jth DUE. From the reward function defined above, learning can be implemented independently in a decentralised manner such that each agent maintains a local Q-table. There is no information exchange relating to other agents' actions or rewards and no cooperation is needed between the agents, which results in reduced signalling overheads and reduced complexity compared with a centralised Q-learning approach.

IV. PERFORMANCE EVALUATION

The performance of the presented BSA scheme is verified by considering a single-cell network in an industrial scenario. The simulation setup and channel models are summarised in Tables I and II. The network dynamics are captured by generating the channel fading effects randomly. The throughput is the main metric used to evaluate the performances of the algorithms. The performances of BSA are compared with centralised optimisation and the game theoretic Deferred Acceptance (DA) schemes [9].

TABLE I. MAIN SIMULATION PARAMETERS [9]

Parameter	Value
Carrier frequency, f_c	2GHz
System bandwidth	10MHz
Number of resource blocks (RB), K	50
RB bandwidth	180 kHz
Maximum CUE transmit power, $P_{c_i,\max}$	23dBm
Maximum DUE transmit power, $P_{d_j,\max}$	13dBm
D2D distance, L_{d_T,d_R}	$10m \leq L_{d_T,d_R} \leq 20m$
CUE SINR Threshold, $\Gamma_{c_i,\min}$	7 dB
DUE SINR Threshold, $\Gamma_{d_j,\min}$	3 dB
Noise power density	-174 dBm/Hz
Number of CUEs, N	50
Number of DUEs, M	50
Reliability for DUE, p_{R_0}	10^{-5}
Exploration rate, ε	0.7
Learning rate, σ	0.9
DUE Maximum Delay, $l_{d_j,\max}$	50ms
DUE Message Size, B_{d_j}	15kB

TABLE II. CHANNEL MODEL FOR LINKS [9]

Parameter	In-factory DUE link	UE-UE link	BS-UE link
Pathloss model	$36.8\log_{10}(d[m] + 35.8$	$40\log_{10}(d[m]) + 28$	$37.6\log_{10}(d[m] + 15.3$
Shadowing	4dB	6dB	8dB
Fast fading	Rayleigh Fading	Rayleigh Fading	Rayleigh Fading

The throughput performance of matched DUEs as a function of the number of DUEs in the system M, is shown in Fig. 1. It can be concluded that the sum throughput of the DUEs increases with the number of cellular users M for all the considered algorithms. As expected, the number of admitted DUEs increases with the introduction of new DUEs to the system but remains unchanged if a valid cellular resource-sharing partner cannot be found because the minimum QoS requirements are not satisfied.

The centralised optimisation and BSA approaches are comparable, while the DA method shows the least performance. The BS-A algorithm outperforms the DA algorithms by up to 9.69% increase in the DUE throughput performance. However, it is semi-distributive as the final resource allocation is implemented by the BS whereas the DA approach is decentralised (the channel selection is user-centric with no BS intervention to achieve autonomy). Players can make their resource allocations choices to maximise their individual and ultimately achieve system stability.

The performance of the sum throughput of the matched UEs (that is valid pairings between CUEs and DUEs) with respect to the number of cellular users M is presented in Fig. 2. The sum throughput increases with M. The BS-A approach shows better performance at $M \leq 35$ with up to 12.05% increase in sum throughput compared to the centralised approach while the centralised approach performed better at $M > 35$ with up to 9.39% increase in throughput. The DA algorithm again shows the least performance with up to 11.29% decrease compared with the BS-A technique. The effect of the outage probability of the p_{R_0}, and delay threshold of the DUEs $l_{d_j,\max}$ on the sum rate of the matched UEs for all algorithms is shown in Fig. 3 and Fig. 4. The sum throughput of the matched UEs increases with p_{R_0} and $l_{d_j,\max}$. This is because higher p_{R_0} causes the interference from the CUEs to be more tolerable by the DUEs, therefore making potential CUE-DUE pairing possible. Similarly, higher $l_{d_j,\max}$ increases the sum throughput at fixed outage probability and payload since the delay requirement is less stringent. More DUEs are able to satisfy the delay constraint and the number of admitted DUEs are increased.

V. CONCLUSION AND FUTURE WORK

We presented a semi-distributed Base Station Assisted (BSA) scheme for Radio Resource Management (RRM) of a network with D2D and cellular users, targeting wireless industrial scenarios. The reinforcement learning based

approach relies on distributed training of the D2D agents. Subsequently, the look-up tables for the D2D agents are loaded to the base station for centralised channel allocation. Simulation results show that the throughput of the presented approach is comparable to traditional centralised optimisation and demonstrates an improved performance relative to the deferred acceptance (DA) scheme. The future work will focus on evaluating the trade-off between performance, complexity and signaling overheads for the BSA scheme relative to other techniques.
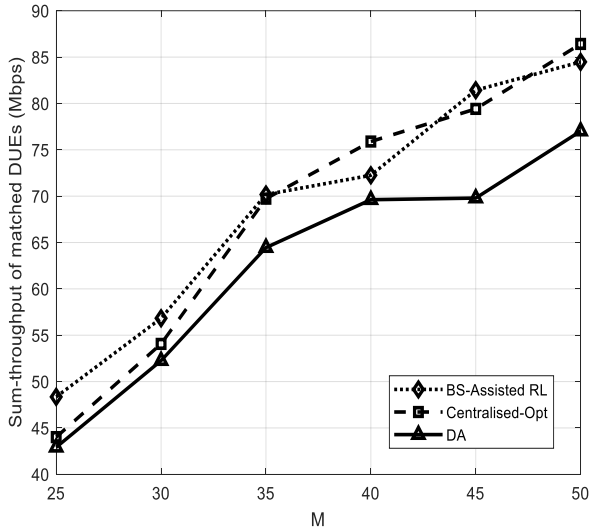
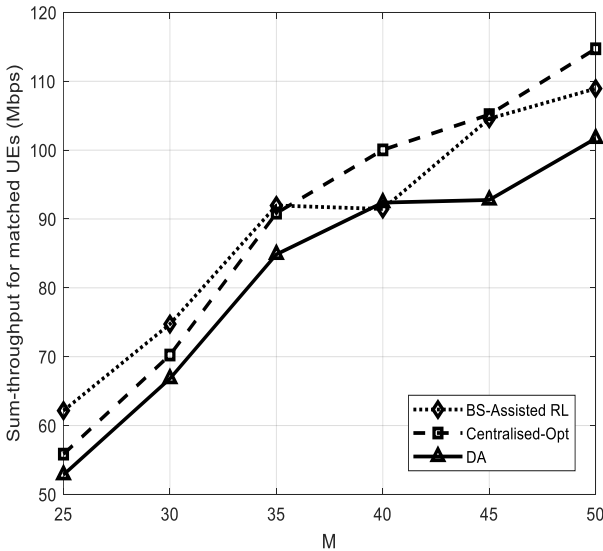Fig. 1. Sum-rate of matched DUEs with varying number of DUEs, M in the System, for $N = 50$

Fig. 2. Sum Throughput of matched UEs as a function of the number of DUEs M, in the system, for $N = 50$
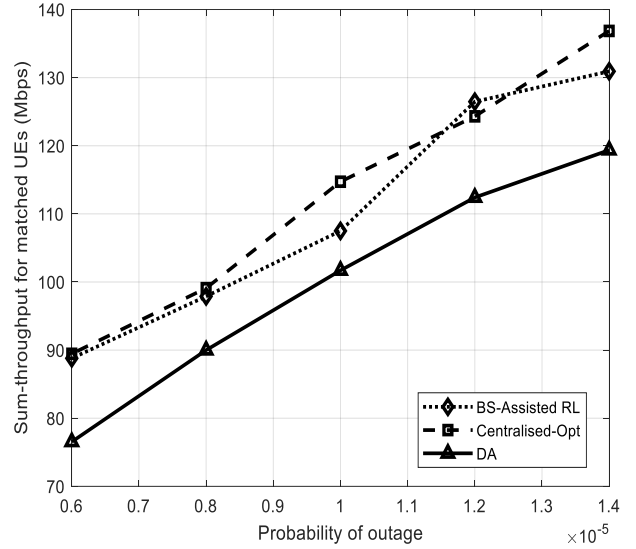
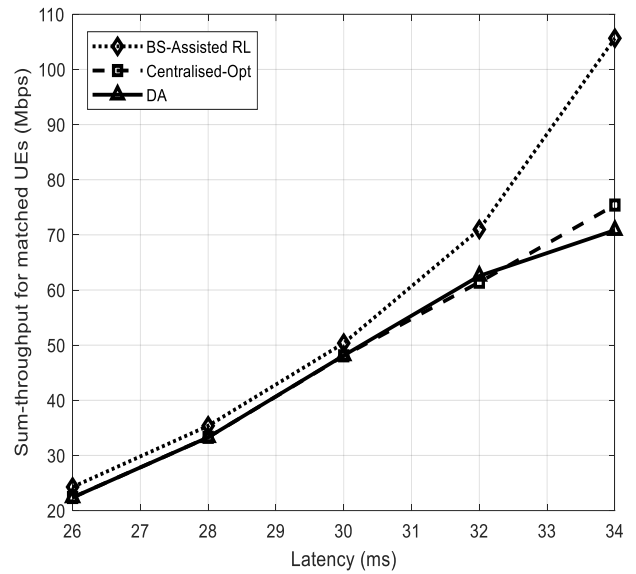Fig. 3. Effect of the DUE outage ratio p_{R_0}, on the sum throughput for $N = M = 50$, $l_{d_j,\max} = 50$ms

Fig. 4. Effect of the delay bound, $l_{d_j,\max}$ on the sum throughput of matched CUE-DUE pair for $N = M = 50$, $p_{R_0} = 10^{-5}$

REFERENCES

[1] J. Wan et al., "Toward dynamic resources management for IoT-based manufacturing," IEEE Communications Magazine, vol. 56, no. 2, pp. 52-59, Feb. 2018.

[2] O.N. Yilmaz et al., "Analysis of ultra-reliable and low-latency 5G communication for a factory automation use case," in Proc. of 2015 IEEE International Conference on Communication Workshop (ICCW), pp. 1190-1195, Sep. 2015.

[3] N. Brahmi, O. N. Yilmaz, K. W. Helmersson, S. A. Ashraf and J. Torsner, "Deployment strategies for ultra-reliable and low-latency communication in factory automation," in Proc. of 2015 IEEE Globecom Workshops (GC Wkshps), pp. 1-6, Feb. 2016.

[4]   Z. Li and C. Guo, "Multi-agent deep reinforcement learning based spectrum allocation for D2D underlay communications," IEEE Transactions on Vehicular Technology, vol. 69, no. 2, pp. 1828-1840, Dec. 2019.

[5]   A. Asheralieva and Y. Miyanaga, "An autonomous learning-based algorithm for joint channel and power level selection by D2D pairs in cellular networks," IEEE transactions on communications, vol. 64, no. 9, pp. 3996-4012, Jul. 2016.

[6]   Z. Li and C. Guo, "Multi-agent deep reinforcement learning based spectrum allocation for D2D underlay communications," IEEE Transactions on Vehicular Technology, pp. 1828-1840, Feb, 2020.

[7]   S. Nie, Z. Fan, M. Zhao, X. Gu and L. Zhang, "Q-learning based power control algorithm for D2D communication," in Proc. of   IEEE 27th Annual International Symposium on Personal, Indoor, and Mobile Radio Communications (PIMRC), pp. 1-6, Sep. 2016.

[8]   K.   Zia et al., "A distributed multi-agent RL-based autonomous spectrum allocation scheme in D2D enabled multi-tier HetNets". IEEE Access, no.7, pp. 6733-6745, Jan. 2019.

[9]   I.O. Sanusi, K.M. Nasr and K. Moessner, "Radio resource management approaches for reliable Device-to-Device (D2D) communication in wireless industrial applications," IEEE Transactions of Cognitive Communication and Networking, vol. 7, no. 3, pp.905-916, Oct. 2021.

[10] L. Liang, H. Ye and G.Y. Li, "Spectrum sharing in vehicular networks based on multi-agent reinforcement learning," IEEE Journal on Selected Areas in Communications, vol. 37, no. 10, pp. 2282-2292, Aug. 2019.

[11] A.T. Kasgari and W. Saad, "Model-free ultra-reliable low delay communication (URLLC): A deep reinforcement learning framework," in Proc. IEEE International Conference on Communications (ICC), pp. 1-6, May 2019.

[12] H. Wang and X. Chu, "Distance-constrained resource-sharing criteria for device-to-device communications underlaying cellular networks," Electronics letters, vol. 48, no. 9, pp. 528-530, Apr. 2012.

[13] H. Yang, X. Xie and M. Kadoch, "Intelligent resource management based on reinforcement learning for ultra-reliable and low-delay IoV communication networks," IEEE Transactions on Vehicular Technology, vol. 68, no. 5, pp. 4157-4169, Jan. 2019.

[14] F.E. Souhir, A. Belghith and F. Zarai, "A reinforcement learning-based radio resource management algorithm for D2D-based V2V communication," in Proc. 15th International Wireless Communications & Mobile Computing Conference (IWCMC), pp. 1367-1372, Jun. 2019.

[15] Z. Li and C. Guo, "Multi-agent deep reinforcement learning based spectrum allocation for D2D underlay communications," IEEE Transactions on Vehicular Technology, pp. 1828-1840, Feb. 2020.

[16] S. Nie, Z. Fan, M. Zhao, X. Gu and L. Zhang, "Q-learning based power control algorithm for D2D communication," in Proc. of   IEEE 27th Annual International Symposium on Personal, Indoor, and Mobile Radio Communications (PIMRC), Sep. 2016.

[17] Y. Wei, Y. Qu, M. Zhao, L. Zhang and F.R. Yu, "Resource allocation and power control policy for Device-to-Device communication using multi-Agent reinforcement learning," Computers, Materials & Continua, vol. 63, no. 3, pp.1515-1532, May 2020.

[18] J. Kim, J. Park, J. Noh and S. Cho, "Autonomous power allocation based on distributed deep learning for device-to-device communication underlaying cellular network," IEEE Access, Vol. 8, 107853-107864, Jun. 2020.